

Shock-heating of stellar envelopes: A possible unifying mechanism at the origin of explosions and eruptions in massive stars

Luc Dessart^{1*}, Eli Livne², and Roni Waldman²

¹ *Laboratoire d'Astrophysique de Marseille, France*

² *Racah Institute of Physics, The Hebrew University, Jerusalem, Israel*

Accepted . Received

ABSTRACT

Observations of transient phenomena in the Universe reveal a spectrum of mass-ejection properties associated with massive stars, covering from Type II/Ib/Ic core-collapse supernovae (SNe) to giant eruptions of Luminous Blue Variables (LBV) and optical transients. In this work, we hypothesize that a large fraction of these phenomena may have an explosive origin, the distinguishing ingredient being the ratio of the prompt energy release E_{dep} to the envelope binding energy E_{binding} . Using one-dimensional one-group radiation hydrodynamics and a set of 10–25 M_{\odot} massive-star models, we explore the dynamical response of a stellar envelope subject to a strong, sudden, and deeply-rooted energy release. Following energy deposition, a shock *systematically* forms, crosses the progenitor envelope on a day timescale, and breaks-out with a signal of hour-to-days duration and a 10^5 – 10^{11} L_{\odot} luminosity. We identify three different regimes, corresponding to a transition from dynamic to quasi-static diffusion transport. For $E_{\text{dep}} > E_{\text{binding}}$, full envelope ejection results with a SN-like bolometric luminosity and kinetic energy, modulations being commensurate to the energy deposited and echoing the diversity of Type II-Plateau SNe. For $E_{\text{dep}} \sim E_{\text{binding}}$, partial envelope ejection results with a small expansion speed, and a more modest but year-long luminosity plateau, reminiscent of LBV eruptions or so-called SN impostors. For $E_{\text{dep}} < E_{\text{binding}}$, we obtain a “puffed-up” star, secularly relaxing back to thermal equilibrium. In parallel with gravitational collapse and Type II SNe, we argue that the thermonuclear combustion of merely a few $0.01 M_{\odot}$ of C/O could power a wide range of explosions/eruptions in loosely-bound massive stars, as those in the 8–12 M_{\odot} range, or in more massive ones owing to their proximity to the Eddington limit and/or critical rotation.

Key words: radiation hydrodynamics – stars: atmospheres – stars: supernovae – stars: transients

1 INTRODUCTION

Stellar explosions, broadly referred to as supernovae (SNe), are understood to stem from a sudden release of energy either associated with the collapse of the degenerate core of a massive star or from the thermonuclear combustion of fresh fuel deep inside the stellar envelope. Whether one or the other mechanism occurs seems to depend on the main-sequence mass of the progenitor star, with core collapse occurring systematically if its value is above $\sim 8 M_{\odot}$ (Woosley et al. 2002, hereafter WHW02). Interestingly, whatever the mechanism, the typical kinetic energy of SN ejecta is on the order of 10^{51} erg, as inferred for example for the well-studied SN 1987A (Type II peculiar; Blinnikov et al. 2000), for SN 1999em (Type II-Plateau, hereafter II-P; Utrobin 2007), or for the very uniform set of events that Type Ia SNe constitutes (Woosley et al. 2007b). The cause of this apparent degeneracy in explosion energy

is, paradoxically, perhaps not so much tied to the mechanism itself, but instead to the rather uniform total envelope binding energy of the progenitor stars, on the order of 10^{51} erg; anything falling short of that leads to a fizzle and no SN display.

The last decade of observations of such transient phenomena has shown, however, that the radiative signatures associated with SNe (as classified in circulars) are very diverse, from very faint to very luminous, from fast-evolving to slow-evolving or fast-expanding to slow-expanding. This diversity has been observed little in Type Ia SNe, with a few peculiar events such as SN 2002ic (presence of narrow hydrogen lines in an otherwise standard Type Ia spectrum; Hamuy et al. 2003) or SNLS-03D3bb (possible Type Ia SN from a super-Chandrasekhar white dwarf star; Howell et al. 2006). In contrast, there has been a rich diversity in explosions associated (perhaps erroneously at times) with massive stars and the mechanism of core collapse. We have observed 1) Type Ic SNe, associated or not with a long-soft γ -ray burst, and with a standard or a very large kinetic energy (SN 1998bw, Woosley et al.

* E-mail: Luc.Dessart@oamp.fr

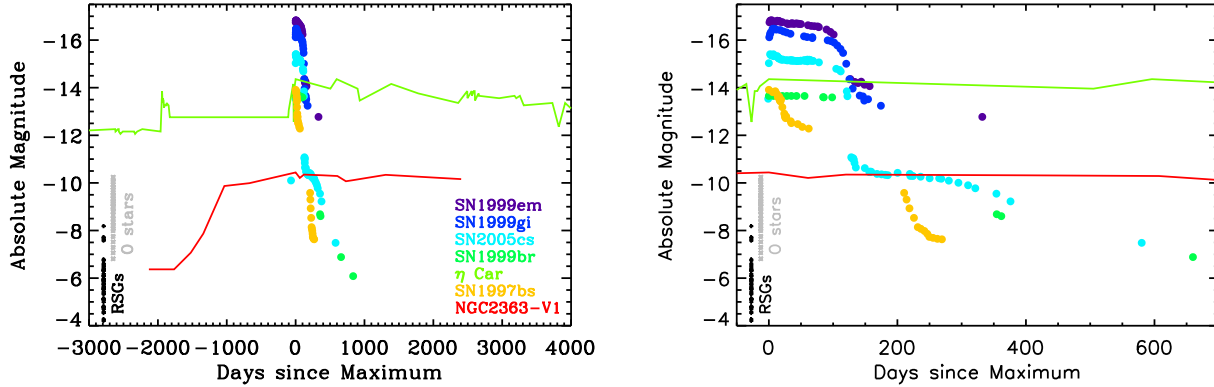


Figure 1. *Left:* Comparison of absolute- V -band-magnitude light curves for a representative sample of SNe, SN impostors and/or erupting LBVs (violet: SN1999em, Leonard et al. 2002a; Dessart & Hillier 2006; blue: SN1999gi, Leonard et al. 2002b; turquoise: SN 2005cs, Pastorello et al. 2009; green: SN1999br, Pastorello et al. 2009; light green: η Car, Frew 2004; yellow: SN 1997bs, Van Dyk et al. 2000; red: NGC2363-V1, Drissen et al. 2001; Petit et al. 2006). For each, we adopt the distance and reddening given in the associated references. The time origin is that of maximum recorded brightness. Note that all these objects have comparable effective temperatures on the order of 10,000 K, hence comparable bolometric correction, making the comparison of their absolute V -band magnitude meaningful. We also show on the left side and in black the absolute visual magnitude of the galactic red-supergiant stars studied by Levesque et al. (2005, black), as well as the *bolometric* magnitude of the O star models computed by Martins et al. (2005, gray; we use the bolometric magnitude here since O stars are hot and have large bolometric corrections). *Right:* Same as left, but now zooming in on the time of maximum brightness (the color coding is the same as in the left panel). Notice the stark contrast between SN light curves, associated with shorter/brighter events, and erupting massive stars, associated with longer/fainter events. Importantly, notice the overlap between the intrinsic brightness of η Car and that of the low-luminosity Type II-P SN 1999br. In this work, we propose that this diversity of radiative displays may be accommodated by a *common, explosive, origin*.

1999; SN 2002ap, Mazzali et al. 2002); 2) a large population of Type II-Plateau (II-P) SNe in what seems to be the generic explosion of a moderate-mass red-supergiant (RSG) star (e.g. SN 2005cs, Maund et al. 2005; Utrobin & Chugai 2008); 3) a growing number of low-luminosity SNe that share properties with standard Type II-P SNe except for being significantly and globally less energetic (e.g. SN1997D, Chugai & Utrobin 2000; SN 1999br, Pastorello et al. 2004; OT2006-1 in M85, whose status is ambiguous, see Kulkarni et al. 2007; Pastorello et al. 2007). We show a sample of V -band absolute-magnitude light curves of such core-collapse SNe in Fig. 1, with representative peak values of -14 to -17 mag and a 100-day plateau duration (best seen in the right panel of that figure), hence about 6-10 mag brighter than their proposed RSG progenitors (shown as black crosses). From this expanded SN sample, the range of corresponding explosion energies has considerably widened, extending above and below the standard 10^{51} erg value. Within the core-collapse SN context, this modulation is thought to stem from modulations in the energy revival of the stalled shock above the nascent proto-neutron star, in turn modulated by the stellar-core structure (Burrows et al. 2007b).

The stretching to low explosion energies of potential core-collapse SN events is intriguing. For the most energetic explosions belonging to points 1 and 2 above, the classification as a SN is unambiguous. However, some transient events show an ejecta/outflow kinetic energy and a peak magnitude that are SN-like, although the events did not stem from core collapse (a star is observed at that location on post-explosion/eruption images); the community calls these SN impostors. Conversely, this raises the issue whether *low-energy* Type II-P SNe are associated with core collapse - they might but they need not. We illustrate this overlap in radiative properties for a sample of such objects in Fig. 1. One such case is the Luminous Blue Variable (LBV) η Car, whose properties during its 1843 eruption rival those of the low-luminosity Type II-P SN1999br. η Car survived this gigantic eruption, which shed about

$10 M_{\odot}$ of material in what now constitutes the homunculus nebula (Smith et al. 2003). In contrast to core-collapse SNe, such eruptive phenomena in massive stars have been associated with the proximity of the star to the Eddington luminosity $L_{\text{Edd}} = 4\pi cGM/\kappa$ (κ is the mass absorption coefficient). Due to the steep dependence of luminosity to mass (e.g. with an exponent of 3.5 for main-sequence objects), this limit is easily reached by very massive stars such as η Car. In this context, massive stars are thought to undergo considerable mass loss when their luminosity overcomes the Eddington limit,¹ giving rise to a porosity-modulated continuum-driven outflow (Shaviv 2000; Owocki et al. 2004). Here, this super-Eddington wind constitutes a quasi steady-state outflow, and has therefore been thought to be of a fundamentally different nature from core-collapse SNe. And indeed, one refers to a wind for the former and to an ejecta for the later. This dichotomy has been exacerbated by the stark contrast in typical light curves of eruptive stars (long lived with large brightness) and core-collapse SN explosions (short lived with huge brightness). In Fig. 1, we show two known eruptive massive stars that highlight this contrast.

However, recent observations may be challenging such a strict segregation. First, the recent identification of very fast outflowing material ahead of η Car's homunculus now suggests that such material was accelerated by a shock, rather than driven in a quasi-steady wind, and thus connects the giant outburst to an explosive origin (Smith 2008). Second, the existence of interacting SNe tells us that a massive eruption can occur merely a few years before explosion. For some, e.g. SN 2006gy (Smith et al. 2007; Smith & McCray 2007; Woosley et al. 2007a) or SN 1994W (Dessart et al. 2009), the amount is thought to be large enough to decelerate the energetic (and necessarily faster-expanding) subsequent ejection. This

¹ Note, however, that energy will have to be supplied to the stellar envelope to push it over this limit, and in large amounts to explain such a nebula as the homunculus.

very strict timing of merely a few years, *which is orders of magnitude smaller than evolutionary or transport timescales*, suggests a connection between the mechanisms at the origin of the two ejections. For SN2006gy, Woosley et al. propose recurrent pair-instability pulsations, a mechanism germane to super-massive stars and therefore extremely rare. For lower mass massive stars, this short delay of a few years seems to exclude a very-long, secular, evolution for the production of the first ejection since this would have no natural timing to the comparatively instantaneous event of core collapse. Motivated by these recent observations, we explore in this paper whether this diversity of events could be reproduced by a unique and deeply-rooted mechanism, associated with the sudden energy release above the stellar core and the subsequent shock heating of the progenitor envelope. This means would communicate a large energy to the stellar envelope on a shock crossing time scale of days rather than on a very long-diffusion time of thousands of years or more. Although different in their origin, this energy release could be a weak analogue of what results in pair-instability pulsations, i.e. a nuclear flash, as identified in the 8-12 M_{\odot} range by Weaver & Woosley (1979).

In this paper, following this shock-heating hypothesis, we use 1D radiation-hydrodynamics simulations to explore the production of explosions/eruptions in stars more massive than $\sim 10 M_{\odot}$ on the main sequence. We parameterize the problem through a simple energy deposition, taking place with a given magnitude, over a given time, and at a given depth in a pre-SN progenitor star. We do not aim at reproducing any specific observation but, through a systematic approach, try to identify important trends, in a spirit similar to that of Falk & Arnett (1977). However, we depart from these authors by studying “non-standard” explosions. In practice, we consider cases where the energy deposited can be both smaller or larger than the binding energy of the overlying envelope, but must imperatively be released on a very short time scale to trigger the formation of a shock. Doing so, we identify three regimes, with “standard” SN explosions (short-lived transients) at the high energy end, objects that we will group in the category SN “impostors” (long-lived transients) at intermediate energy, and variable stars at the very low energy end. Let us stress here that we do not make the claim that all massive-star eruptions, or all transients in general, stem from a strong, sudden, and deeply-rooted energy release in their envelope. Here, we make this our working hypothesis and investigate how much such an explosive scenario can explain observations. We do find that this scenario has great potential and should be considered as a possibility when examining the origin of massive-star eruptions and associated transient phenomena.

The paper is structured as follows. In §2, we briefly present the stellar evolutionary models of WHW02 that we use as input for our 1D 1-group radiation-hydrodynamics simulations. We discuss the properties of the progenitor massive stars of WHW02, such as density structure and binding energy, that are relevant for the present study. We then describe in §3, the numerical technique and setup for our energy deposition study. In §4, we present the results of a sequence of simulations based primarily on the 11 M_{\odot} model of WHW02, discussing the properties of the shocked progenitor envelope for different values of the strength (§4.1), the depth (§4.2) and the duration (§4.3) of the energy deposition. We also discuss in §4.4 the results obtained for more massive pre-SN progenitors, ranging from 15 to 25 M_{\odot} on the main sequence. In §5, we present synthetic spectra computed separately with CMFGEN (Hillier & Miller 1998; Dessart & Hillier 2005b; Dessart et al. 2009) for a few models at a representative time after shock breakout. In §6, we discuss the implications of our results

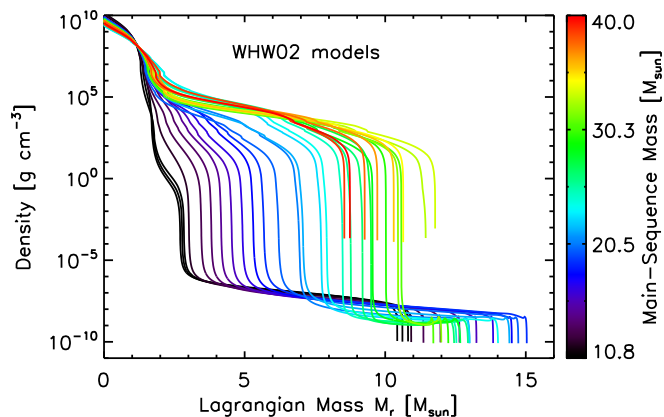


Figure 2. Density distribution as a function of Lagrangian mass at the onset of collapse for the models of WHW02 evolved at solar metallicity. Notice the flattening density distribution above the core for increasing mass. In low-mass massive stars, the star is structured as a dense inner region (the core), and a tenuous extended H-rich envelope.

for understanding transient phenomena, and in §7 we summarize our conclusions.

2 INPUT STELLAR EVOLUTIONARY MODELS AND PHYSICAL CONTEXT

2.1 Input Models

The energy-deposition study presented here starts off from the stellar evolutionary calculations of WHW02, who provide a set of pre-SN massive stars, objects evolved all the way from the main sequence until the onset of core collapse. We refer the reader to WHW02 for a discussion of the physics included in such models. These physically-consistent models give envelope structures that obey the equations and principles of stellar structure and evolution. The exact details of these models are not relevant since we aim at developing a general, qualitative, understanding of stellar envelope behaviour in response to shock-heating - we do not aim at connecting a specific observation to a specific input. Here, we focus on 10-40 M_{\odot} progenitor stars evolved at solar metallicity and in the absence of rotation. These calculations include the effect of radiation-driven mass loss through a treatment of the outer-boundary mass-flux, so that the final mass in this set reaches a maximum of $\sim 15 M_{\odot}$ for a $\sim 20 M_{\odot}$ progenitor star. Mass loss leads also to a considerable size reduction of the stellar envelope, with partial or complete loss of the hydrogen rich layers, producing smaller objects at core collapse for main-sequence masses above $\sim 30 M_{\odot}$. In the sequence of pre-SN models of WHW02, surface radii vary from 4–10 $\times 10^{13}$ cm in the 10-30 M_{\odot} range, decreasing to $\sim 10^{11}$ cm in the 30-40 M_{\odot} range.

The density distribution above the iron core is an important property that distinguishes the structure of massive stars. Low-mass massive stars show a steep density fall-off above their degenerate core, while the more massive stars boast very flat density profiles (Fig. 2; recall that at the time shown, the Fe or ONeMg core is degenerate and starts to collapse). In the context of core-collapse SN explosions, this has been recognized as one of the key aspect of the problem, since this density profile directly connects to the mass-accretion rate onto the proto-neutron star in the critical first second that follows core bounce (Burrows et al. 2007b). This has led

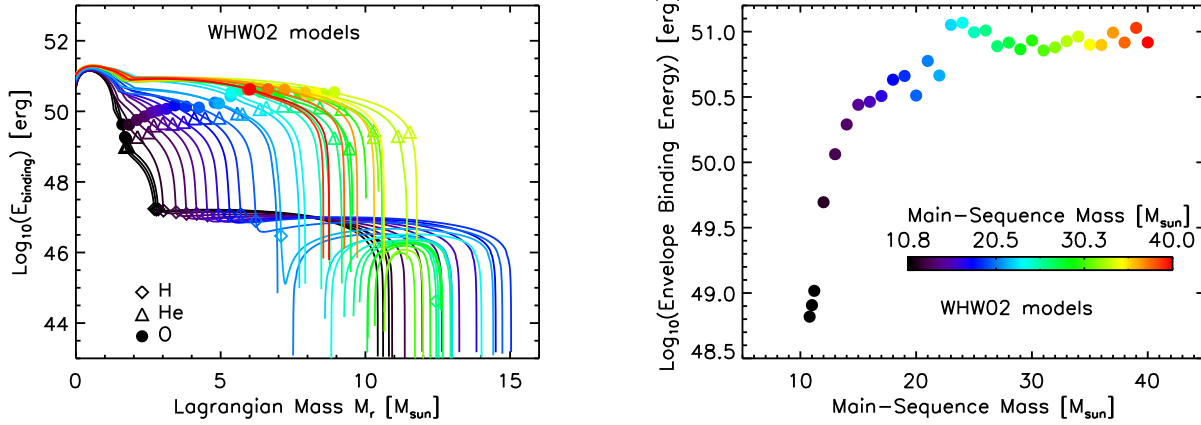


Figure 3. *Left:* Same as Fig. 2, but now for the binding energy as a function of the Lagrangian-mass coordinate M_r of the envelope exterior to M_r : $e_{\text{binding}}(M_r) = \int_r^{r_{\text{max}}} (GM_r/r - e_{\text{int}}) dM_r$. In our determination of the binding energy, we have included the internal energy (Zeldovich & Novikov 1971). Symbols refer to the base of the corresponding shells, with diamond for the H-rich shell, triangles for the He-rich shell, and dots for the O-rich shell. *Right:* Variation of the envelope binding energy at the onset of collapse in the models of WHW02 and shown as a function of the progenitor mass on the main sequence. Here, the “envelope” refers to total mass exterior to the inner $1.8 M_{\odot}$. The colorbar applies to both left and right panels.

Burrows & Goshy (1993), and more recently Murphy & Burrows (2008) to identify a criterion for explosion through a competition between neutrino luminosity and mass accretion rate. Such a criterion, although tuned by the global hydrostatic configuration of the progenitor star, isolates the conditions for a successful explosion to those in the direct vicinity of the pre-collapsed core. A more global, and more fundamentally meaningful, criterion for a successful explosion is whether the energy deposited at the base of the progenitor envelope is smaller or greater than its binding energy. This matter is rarely addressed explicitly, supposedly because the 10^{51} erg explosion energy aimed for is thought to be much in excess of the binding energy of the envelope, but this may in fact not be the case and it is ignoring the key role the binding energy plays in producing the diversity of characters observed in core-collapse SNe, and potentially in numerous transients.

2.2 The Binding Energy Barrier

The variation in the progenitor envelope density structure (Fig. 2) is echoed in the corresponding binding energy of the stellar envelope. In the left panel of Fig. 3, we show the binding energy of the envelope exterior to a Lagrangian-mass coordinate M_r , as a function of M_r , for the same set of pre-SN massive star models. To differentiate mass shells of different compositions, we use symbols to mark the inner edge of the hydrogen shell (diamond), of the He-rich shell (triangle), and of the O-rich shell (dot). The binding energy shows a strong dependency with progenitor main-sequence mass, and we can identify two classes of objects. Objects with main-sequence mass below $\sim 25 M_{\odot}$ possess a sizable hydrogen envelope, whose fraction of the total mass at the onset of collapse grows as we go to lower-mass progenitors. It represents at collapse $\sim 80\%$ of the total mass in the $11 M_{\odot}$ model, but only $\sim 30\%$ in the $25 M_{\odot}$ model (these masses refer to the main-sequence mass). In all these cases, whenever present, the binding energy of the hydrogen shell is very small, on the order of 10^{47} erg, hence very loosely bound to the star. In contrast, for objects with main-sequence masses in excess of $25\text{--}30 M_{\odot}$, the hydrogen envelope is shed through mass loss during the pre-SN evolution, and the pre-SN star is essentially a “compact” star, with an envelope whose binding energy is now

3–4 orders of magnitude larger. This is perhaps the single-most important characteristics of pre-SN massive star envelopes, namely that hydrogen-deficient (generally higher-mass originally) stars are very tightly-bound objects while hydrogen-rich (generally lower-mass originally) stars are very loosely bound.

Moving deeper into the envelope, i.e. in the He or O shells, the same trend persists, with a systematic increase in binding energy for each shell edge as we move up in mass from low-mass to high-mass massive stars. As shown in the right panel of Fig. 3, the binding energy of the entire envelope exterior to the degenerate core varies from $\lesssim 10^{49}$ erg for the $11 M_{\odot}$ model (a RSG star with a final mass of $\sim 10.6 M_{\odot}$) up to $\sim 10^{51}$ erg in the $40 M_{\odot}$ (a H-deficient Wolf-Rayet star with a final mass of $\sim 8 M_{\odot}$) model.

For an explosion to ensue, an energy greater than the binding energy must be deposited suddenly at the base of the envelope, the excess energy above the binding energy being used to accelerate the envelope and turn it into outflow/ejecta. While a very modest energy of $\sim 10^{49}$ erg is sufficient to unbind the envelope of a $10 M_{\odot}$ RSG star, such a deposition in a Wolf-Rayet star would produce nothing remarkable. In the present work, the connection between energy deposition and binding energy is key to the understanding of the properties of the resulting mass ejections. More generally, the low binding energy of massive star envelopes is of primary importance for the understanding of their stability/variability, as in the context of pulsations, for example.

The origin of the energy deposition that we artificially treat in this work may be a sequel of the gravitational collapse of the core, in which case it can happen only once, leading either to an explosion or to a fizzle. Alternative sources in massive stars will likely be less energetic, but in objects with low binding energy, may still be of relevance to a wide spectrum of astrophysical events. The most suited mechanism in the present context would be the prompt thermonuclear combustion of a small amount of already processed material, like carbon, oxygen, or silicon, at a location just above the degenerate core. Such “nuclear flashes” have indeed been encountered in stellar-evolutionary calculations of $8\text{--}12 M_{\odot}$ massive stars (Weaver & Woosley 1979). Interestingly, with a (nuclear) binding energy of ~ 1 MeV/nucleon, the combustion of ^{12}C or ^{16}O to ^{56}Fe liberates $E_{\text{nuc}} \sim 1.9 \times 10^{49} (M/0.01 M_{\odot})$ erg. Hence, as little as

a few percent of a solar mass of carbon or oxygen burnt to iron can yield an energy in excess of the binding energy of the lowest-mass massive stars, and of comparable magnitude to that of the weakest core-collapse SN explosions (Pastorello et al. 2004; Kitaura et al. 2006) or LBVs.

2.3 Energy Transport by Diffusion/Convection versus Shock-heating

In radiative stellar envelopes, energy is transported outward by diffusion. Any increase in energy release from the core provokes a steepening of the temperature profile and an enhanced radiative flux, carrying outward this extra energy, often aided by convection too. However, radiative diffusion or convection can only be effective for small increases in energy, due to the short mean-free path of photons and/or the modest sound speed. Associated time scales for such energy transport are therefore long and the means poorly efficient. In Fig. 4, we show the diffusion time as a function of depth in the 10–40 M_{\odot} model sequence of WHW02, computed by adopting a constant mass-absorption coefficient of $0.1 \text{ cm}^2 \text{ g}^{-1}$ (intermediate between that for the hydrogen-rich and silicon-rich shells) but a depth-dependent mean-free-path (Mitalas & Sills 1992, this is controlled primarily by the twenty-order-of-magnitude variation in density between the core and the surface). Resulting diffusion times from regions immediately above the core range from 10^4 to 10^5 years. In contrast, the shock crossing time scale of the envelope is $\sim R_*/\langle v_{\text{shock}} \rangle$, which for Wolf-Rayet to RSG progenitor stars with radii of 10^{11} to 10^{14} cm and even modest, but supersonic, shock waves with $\langle v_{\text{shock}} \rangle \sim 1000 \text{ km s}^{-1}$, is typically on the order of days.

In this study, we want to explore what happens when the deposition of energy leads to an energy increase that cannot be remedied either by diffusion or convection transport, but instead has to lead to shock formation (even for small energy deposition). This leads to a completely different regime since in this situation the shock can communicate this extra energy to the *entire* envelope on a short timescale of days: The stellar envelope hence responds immediately to the change of conditions at depth, instead of secularly evolving to a bigger/smaller or cooler/hotter star. This dichotomy was recently discussed in the context of the helium flash, whose associated energy was found to be too small to lead to the formation of a shock (Mocák et al. 2008, 2009). In our artificial approach, the energy release has to occur on a very short time scale to trigger the formation of a shock. How short will depend on the progenitor since, as shown in Fig. 5, the depth-dependent internal energy (including both radiation and thermal components) varies considerably between progenitors, increasing at a given M_r with main-sequence mass. Forming a shock will require a stronger energy deposition, a shorter deposition time, and/or a more exterior deposition site in higher mass progenitors.

2.4 Origin of energy deposition

In the present study on pre-SN massive-star progenitors, we find that an energy deposition that is marginally larger than the envelope binding energy yields ejecta that are reminiscent of SN impostors, but in the present context, are also reminiscent of the mass ejections that must take place prior to core collapse in interacting SNe. The short delay between the two ejections, of no more than a few years to produce a luminous interacting SN, suggests a shock-heating solution for both ejections. Any other energy-transport means in a

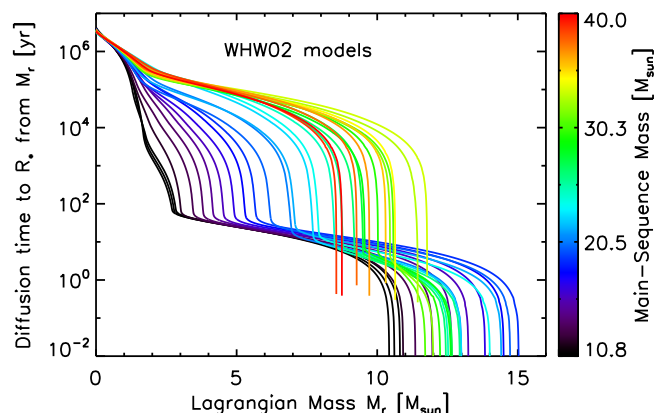


Figure 4. Same as Fig. 2, but now showing the variation of the diffusion time. The computation assumes unequal photon mean-free-path as in Mitalas & Sills (1992), but a constant and representative mass absorption coefficient of $0.1 \text{ cm}^2 \text{ g}^{-1}$.

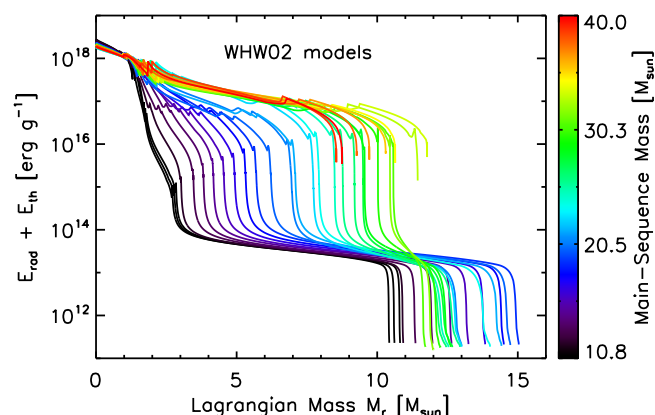


Figure 5. Same as Fig. 2, but now showing the variation of the internal energy (including radiation and thermal parts).

massive star that could propel mass out of the gravitational potential would take place on a timescale of thousands of years or more. The disconnection between the surface and the core thus suggests that both events are tied to a phenomenon that happens in the core or in its direct vicinity. We propose thermonuclear flashes associated with shell burning in the last stages of massive star evolution (pair-instability pulsations are analogous to this scenario but may only apply to stars with a main-sequence mass in the range 95–130 M_{\odot} ; Woosley et al. 2007a). These burning stages are very short (month to year timescales) and always occur at the end of the life of all massive stars. They offer a natural tuning and a reproducible circumstance for the production of interacting SNe, with at least one major interaction between the penultimate shell ejection and that resulting from the gravitational collapse of the degenerate core. Given the relatively large number of interacting SNe compared to the strict time requirements to produce them (a few-year delay is no more than an instant relative to the lifetime of a star!) suggests that indeed the conditions must be met often rather than encountered by chance. The stellar-evolutionary calculations of Weaver & Woosley (1979) for 8–12 M_{\odot} massive stars support the occurrence of nuclear flashes. In this work, we emphasize the dire consequences of such an energy release on loosely-bound massive stars, potentially

triggering single eruptions as evidenced in transients or multiple eruptions as evidenced in interacting SNe (Dessart et al. 2009).

More generally, the hydrodynamical investigations of the late stages of nuclear burning in massive stars by Bazan & Arnett (1994, 1998); Asida & Arnett (2000); Arnett et al. (2005); Meakin & Arnett (2006) reveal the multi-dimensional and time-dependent nature of the problem, issues that have been largely overlooked in stellar evolutionary calculations so far. In particular, they find that considerable energy can leak out of the convectively-burning shells in the form of waves, with a potential to alter the otherwise quasi-steady hydrostatic configuration of the stellar envelope. Similar investigations in the $8\text{--}12\text{ M}_{\odot}$ range are highly needed.

These works provide a physical motivation for our investigations. For the simulations presented here, we do not, however, build a fully-consistent picture of the problem, but instead start off by imposing the modalities of such an energy deposition. In practice, we follow a very simple approach, adopting a constant energy-deposition rate for a given duration. We thus neglect any feedback of the dynamics on the mechanism causing the energy release.

3 NUMERICAL TECHNIQUE AND COMPUTATIONAL SETUP

The numerical simulations presented in this work were all performed with Vulcan/1D (V1D), a one dimensional radiation-hydrodynamics code that works in the framework of Newtonian physics. It incorporates many methods and techniques, using both Lagrangian and Eulerian schemes for planar, cylindrical, and spherical geometries. The Lagrangian hydrodynamics scheme is based on the staggered-grid method described in Richtmyer & Morton (1967), which uses artificial viscosity for shock waves. Some test problems of an early version of this code are described in Livne (1993).

For the treatment of non-LTE radiative-transfer problems we have recently implemented several solvers with different levels of approximations for the radiation fluxes. The coarser method is our gray flux-limited-diffusion method, which has also a multi group extension. We have also constructed more accurate schemes for the radiation fields using moment methods and full angle-dependent solvers, which are similar in nature (but not in details) to the scheme described in Ensman (1991, 1994). Those however were not implemented in this work. The radiation field is coupled to matter in a fully implicit fashion, which guaranties stability and large time steps. Since the important physics relevant to this study occurs at large optical depth, the multi-group capability of the code is not used. Opacities/emissivities are interpolated from a set of tables prepared with a separate program. It computes the populations for a large number of atomic levels (up to 1000 per species), under the assumption of LTE, for typically fifteen species (H, He, C, N, O, Ne, Na, Mg, Si, S, Ar, Ca, Cr, Fe, and Ni), and for a set of compositions representative of the pre-SN envelope of a 15 M_{\odot} main-sequence star (we generate tables for compositions corresponding to a mean atomic weight between 1.3 and 25 atomic-mass units). For each species, up to 18 ionization stages are included. At present, we account for scattering opacity (due to electrons), and absorptive opacity due to bound-free and free-free processes. Although lines can be included, we have neglected them in this study.

The equation of state takes into account excitation/ionization to all available levels of the different atomic/ionic species in the composition. The distribution function of these levels is computed

using a method similar to the one described in Kovetz & Shaviv (1994). The resulting electron density is then used together with the temperature in order to extract the pressure, energy, chemical potential and their derivatives respective to the electron density and temperature from a table computed in advance by solving the Fermi-Dirac integrals. The pressure, energy and entropy of the ions are then added as an ideal gas.

All our simulations use as inputs the massive-star models of WHW02, evolved from the main sequence until the onset of core collapse. At present, V1D adopts the same grid as the one read-in from the chosen input model of WHW02. The resolution is therefore quite low at the progenitor surface, which affects the accuracy of the breakout signal. The range of mass encompassed by the V1D grid is set by the inner mass cut where energy is deposited, the excised region being shrunk to a point mass at the origin. We do not compute the explosive nucleosynthetic yields, and thus do not alter the original composition of the massive-star envelopes computed by WHW02. In particular, there is no production of ^{56}Ni and no associated heating through radioactive decay accounted for in our simulations. In the main parameter study presented here, we use the 11 M_{\odot} model (named s11.0 by WHW02). We first explore the evolution of the progenitor envelope after depositing an energy E_{dep} between 5×10^{48} erg and 1.28×10^{51} erg at a mass cut $M_{\text{cut}} = 1.8\text{ M}_{\odot}$ (uniformly deposited in the range 1.8 to 2.3 M_{\odot}) and for a duration of 10 s (§4.1). We also explore the sensitivity of the outcome to the location of the energy deposition, from a Lagrangian mass coordinate of 1.8 to 3, 7, and 9 M_{\odot} (§4.2), and to the duration of the energy deposition, from ten seconds, to one hour, one day, one week, and one month (§4.3). Finally, we perform a few simulations using more massive progenitors, with 15, 20, and 25 M_{\odot} main-sequence mass (§4.4). A summary of the model initial parameters as well as quantities characterizing the main results is shown in Tables 1 and 2. Note that in the text, when we mention the masses associated with the WHW02 models, we mean the main-sequence masses, as in the 11 M_{\odot} or the 25 M_{\odot} models; these do not correspond to the star mass at the onset of collapse, which is shown for all models in, e.g., Fig. 2.

4 RESULTS FOR THE 11 M_{\odot} SEQUENCE

4.1 Effect of varying the Energy Deposition Magnitude

In this section, we present the results for the sequence of simulations based on the 11 M_{\odot} model for a range of energy deposition magnitudes. A compendium of parameters describing the set up and the results is given in Table 1. Note that, initially (prior to energy deposition), the envelope (total) internal energy is $\sim 10^{49}$ erg, and its gravitational binding energy is -2.2×10^{49} erg in this 11 M_{\odot} model (the model mass at the time of collapse is 10.6 M_{\odot}).

In our simulations, energy deposition leads to a strong increase in internal energy (temperature, pressure), leading to the formation of a shock which moves outward. In all runs, the shock crosses the entire envelope and eventually emerges at the surface of the progenitor, giving rise to a shock-breakout signal (more precisely, a radiative precursor precedes the emergence of the shock, but one generally refers to this whole phase as shock breakout). The shocked envelope left behind has been turned into a radiation-dominated plasma, with an extra energy that varies from a small ($E_{\text{dep}} = 5 \times 10^{48}$ erg in the s11.0 model) to a large value ($E_{\text{dep}} = 1.28 \times 10^{51}$ erg in the s11.8 model).

After energy deposition, all the stored energy is internal. As

Table 1. Summary of the parameters and key results for the sequence started with the $11 M_{\odot}$ progenitor model (pre-SN mass of $10.6 M_{\odot}$). Note that all models are not run for the same total time (t_{end}), owing to numerical problems at very late times as the density and temperature drop in the outer ejecta. Numbers in parenthesis refer to powers of ten in the unit shown in the first column of the same row. The effective mass on the V1D grid depends on the adopted inner mass cut M_{cut} . The time origin corresponds to the start of the simulation, when energy is deposited for t_{dep} seconds. Starting from the top row down, we give the total energy deposited (in 10^{50} erg), the inner mass shell where it is deposited and the duration of that deposition (in s), the time at the end of the simulation (in days), the sum of the mass of all shells that at the end of the simulation have a velocity larger than the local escape speed $\sqrt{2GM_r/r}$, the ejecta mass-weighted average velocity (in km s^{-1}), the kinetic energy of the ejecta (in 10^{50} erg) at the end of the simulations, the maximum ejecta velocity (in km s^{-1}), the time (in days) and the peak luminosity (in L_{\odot}) of shock breakout, the average speed of the shock (in km s^{-1}), the kinetic and the internal (thermal plus radiation contributions) at the time of breakout (in erg), the time of peak luminosity in the post-breakout plateau (in days) and the corresponding luminosity (in L_{\odot}), the duration of high brightness for the transient (time during which the luminosity is greater than $1/50$ th of $L_{\text{peak,plateau}}$), and the time-integrated bolometric luminosity (in 10^{49} erg; note that the time interval varies between models). [See text for discussion.]

Model Name	s11_0	s11_01	s11_1	s11_2	s11_3	s11_4	s11_5	s11_6	s11_7	s11_8
E_{dep} (10^{50} erg)	5.0(-2)	7.5(-2)	1.0(-1)	2.0(-1)	4.0(-1)	8.0(-1)	1.6(0)	3.2(0)	6.4(0)	1.28(1)
M_{cut} (M_{\odot})	1.8	1.8	1.8	1.8	1.8	1.8	1.8	1.8	1.8	1.8
t_{dep} (s)	10	10	10	10	10	10	10	10	10	10
t_{end} (d)	730	193	730	730	160	730	117	103	730	686
M_{ejected} (M_{\odot})	0.13	5.95	7.75	8.60	8.72	8.79	8.80	8.80	8.80	8.80
$\langle v \rangle_M$ (km s^{-1})	42	76	121	296	510	789	1165	1687	2412	3432
$(E_{\text{kin}})_{\text{end}}$ (10^{50} erg)	2.30(-5)	4.00(-3)	1.33(-2)	9.25(-2)	2.79(-1)	6.74(-1)	1.47(0)	3.08(0)	6.30(0)	1.276(1)
$\langle v_{\text{max}} \rangle$ (km s^{-1})	60	410	560	1310	1800	2740	4100	5970	8740	12700
t_{SBO} (d)	54.7	32.1	21.4	9.6	5.8	3.8	2.6	1.8	1.3	0.9
$L_{\text{peak,SBO}}$ (L_{\odot})	1.7(5)	3.3(6)	5.2(7)	1.2(9)	4.9(9)	1.6(10)	4.2(10)	1.1(11)	2.5(11)	5.7(11)
$\langle v_{\text{shock}} \rangle$ (km s^{-1})	86	147	221	492	812	1238	1815	2622	3717	5244
$(E_{\text{kin}})_{\text{SBO}}$ (erg)	2.1(46)	2.1(47)	6.7(47)	4.4(48)	1.3(49)	3.1(49)	6.7(49)	1.4(50)	2.8(50)	5.8(50)
$(E_{\text{int}})_{\text{SBO}}$ (erg)	5.2(48)	4.6(48)	3.8(48)	7.5(48)	1.7(49)	3.9(49)	8.3(49)	1.7(50)	3.5(50)	7.1(50)
$t_{\text{peak,plateau}}$ (d)	208	198	243	115	97	82	73	64	55	49
$L_{\text{peak,plateau}}$ (L_{\odot})	3.6(5)	1.5(6)	2.9(6)	1.2(7)	2.9(7)	6.0(7)	1.1(8)	2.0(8)	3.6(8)	6.2(8)
$\Delta t_{\text{plateau}}$ (d)	675	517	341	287	>155	180	>115	>106	111	100
$\int L_{\text{bol}} dt$ (10^{49} erg)	6.6(-3)	5.6(-3)	2.5(-2)	6.7(-2)	1.3(-1)	2.5(-1)	4.0(-1)	6.6(-1)	1.1(0)	1.8(0)

the shock forms and moves out, that stored internal energy is converted into kinetic energy behind the shock, and as the shock progresses outward, more and more material is shock-heated and the total internal energy goes up at the expense of the kinetic energy. As time progresses further, the kinetic energy eventually increases due to radiation work on the ejecta. Figure 6 illustrates this evolution until just after shock breakout for the case in which $E_{\text{dep}} = 1.6 \times 10^{50}$ erg (model s11_5).

As the shock approaches the surface, the envelope properties become qualitatively and quantitatively different, depending on the adopted E_{dep} value. For a large E_{dep} , we find that at shock emergence, the total envelope energy is in rough equipartition between kinetic and internal. As time progresses, all the energy is eventually converted into kinetic as radiation, nearly entirely trapped at large optical depth, does work to accelerate the ejecta to its asymptotic velocity.

In contrast, for small E_{dep} , the kinetic energy of the envelope at breakout and later is very small. Here, the stored internal energy is weakly enhanced after energy deposition (i.e. $E_{\text{dep}} \lesssim E_{\text{int}}$ originally), and this excess energy is essentially all exhausted in doing work against gravity, merely lifting off the envelope from the gravitational potential well. At shock emergence, the envelope kinetic energy is thus negligible.

Hence, while in all cases from low to high energy deposition, a shock forms and eventually emerges at the progenitor surface, the quantitative differences are very large between cases. Transitioning from dynamic to quasi-static diffusion regimes of energy transport, we identify three situations: 1) The energy deposition is much larger than the binding energy and a SN-like explosion ensues; 2) the energy deposition is on the order of the binding energy

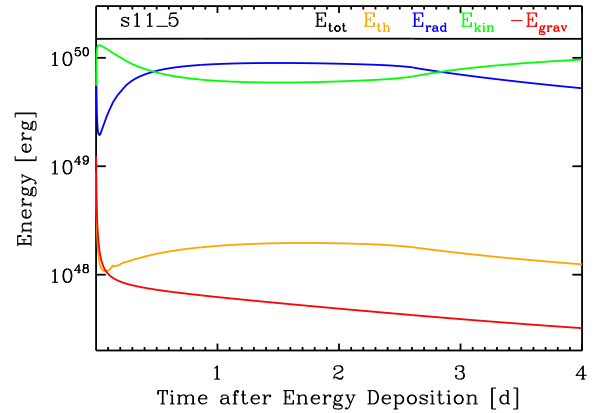


Figure 6. Time evolution of the mass-integrated total (black), thermal (orange), radiative (blue), kinetic (green), and gravitational (red; its absolute value) energies for the model s11_5. Notice the interplay between radiative (which dominates the internal energy over the thermal component) and kinetic energy. The time of shock breakout is 2.6 d, at which the total internal (kinetic) energy is 8.3×10^{49} erg (6.7×10^{49} erg). The time origin is the start of the simulation.

and a low-energy explosion/eruption results; and 3) the energy deposition is lower than the binding energy and the excess energy merely shifts the star to a new quasi-equilibrium state from which it relaxes on a very long timescale. In the following subsections, we describe each of these regimes individually.

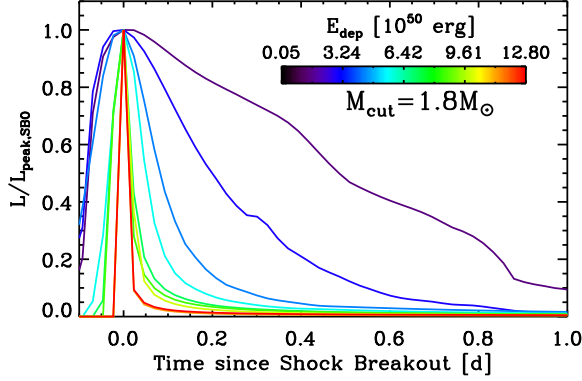


Figure 7. Time evolution of the normalized intrinsic bolometric luminosity around shock breakout, as computed with V1D, and revealing the hour-to-day range in duration of the shock-breakout signal, caused here by the change in shock speed (or explosion energy). Light-travel-time delays are not accounted for. The variation in the breakout-peak luminosity is shown in Fig. 8. A color coding is used to differentiate models.

4.1.1 $E_{\text{dep}} > E_{\text{binding}}$

This regime applies to our simulations with E_{dep} between 4×10^{49} erg (model s11.3) and 1.28×10^{51} erg (model s11.8). The separation between this sample and cases with lower energy deposition is drawn at the threshold value of E_{dep} for which the entire envelope is ejected. In Table 1, we give a census of the properties for this set. Although qualitatively similar, these simulations give rise to $8.8 M_{\odot}$ ejecta with a mass-weighted average velocity in the range $500\text{--}3500 \text{ km s}^{-1}$, and kinetic energy in the range 2.8×10^{49} ($E_{\text{dep}} = 4 \times 10^{49}$ erg) up to 1.276×10^{51} erg ($E_{\text{dep}} = 1.28 \times 10^{51}$ erg). For the former, the binding energy takes a visible share of the energy deposited so that the asymptotic kinetic energy is sizably smaller than E_{dep} . For the latter, the energy deposited is overwhelmingly large and represents 99.7% of the final kinetic energy. In all cases, the initial prompt deposition of energy turns the stellar envelope into a true “ejecta”, and this material is lost from the star without any noticeable fallback.

We find that the shock-crossing time through the envelope is between 0.9 and 5.8 d (the distance between the deposition site and the progenitor surface is 4.7×10^{13} cm), with a time-averaged shock velocity between ~ 5000 and 800 km s^{-1} (in the same order from high to low E_{dep}).² This therefore modulates the delay between the energy release (which may be a sequel of gravitational collapse or otherwise) and the time of shock breakout, which is the first detectable signal testifying for the violent energy deposition that took place at depth. Importantly, this breakout signal is the unambiguous signature that a shock wave emerged from the progenitor surface, a signature that would directly eliminate steady-state wind solutions for the origin of the subsequent outflow/ejecta.

Owing to the sizable range in shock speeds, the breakout signal varies considerably in duration. From a random walk argument, it is born when the decreasing envelope optical-depth τ at the shock depth Δr below the surface eventually makes the diffusion time $t_{\text{diff}} = \tau \Delta r / c$ shorter than the shock-propagation time to the progenitor surface $t_{\text{shock}} = \Delta r / v_{\text{shock}}$. This occurs at an optical depth

$\tau \sim c / v_{\text{shock}}$, and can be very large for a small shock-propagation speed. As shown in Fig. 7 (note that the luminosity in this figure is normalized to the peak value to better illustrate its time variation), we find shock-breakout durations from ~ 0.5 up to ~ 2 hr in the sequence (we refer to the intrinsic breakout duration, hence neglect light-travel time effects which would broaden the signal seen by a distant observer over a duration of at least $\sim R_{\star} / c \sim 1$ hr). Similarly, the peak luminosity at breakout varies enormously with the energy deposited or the shock strength, as shown in the left panel of Fig. 8, where the time axis is the time since energy deposition. To a higher energy-deposition strength corresponds stronger shocks, shorter shock-crossing times (earlier shock emergence), and both shorter-duration and greater peak breakout luminosities. For the range of models discussed in this section, we obtain values between 4.9×10^9 up to $5.7 \times 10^{11} L_{\odot}$, a contrast of about a hundred which is comparable to the corresponding contrast in asymptotic ejecta kinetic energy. So far, the systematics of shock breakout have been tied to variations in the progenitor properties such as surface radius or atmospheric scale height, while obviously the explosion energy, if stretched to low enough values, can lengthen considerably the breakout signal. But importantly, while the delay between energy deposition and breakout varies by a factor of a hundred in this model set, it remains on a timescale of days and hence much shorter than the diffusion time on the order of thousands of years for the corresponding layers (see §2.3).

These properties at and subsequent to breakout are visible in the conditions at the photosphere, which we show in Fig. 9 for the velocity V_{phot} , the radius R_{phot} , the temperature T_{phot} , and the Lagrangian mass coordinate M_{phot} . Because of the infrequent writing of model quantities to file, the breakout phase is not well resolved. This matters little for the velocity, the radius, and the mass at the photosphere, which all evolve slowly. However, the photospheric temperature shows a peak whose strength is underestimated in the high energy-deposition cases, characterized by short breakout durations (note that the low spatial resolution at the progenitor surface prevents an accurate modeling of this breakout phase in any case). Hence, at breakout, we find an approximate range of photospheric temperatures between 5×10^4 to multiples of 10^5 K. In scattering-dominated atmospheres, the color temperature of the emergent spectral-energy distribution corresponds roughly to the gas temperature at the thermalization depth (Mihalas 1978, p 149), which is up to a factor of two greater than T_{phot} (Dessart & Hillier 2005a). For a thermal (blackbody) emitter at T , the peak of the spectral-energy distribution (SED) is at $\sim 2900 / T_4 \text{ \AA}$ (where T_4 is $T / 10^4$ K). At breakout, the spectral-energy distribution for the present set of models will thus peak in the range $100\text{--}600 \text{ \AA}$. It is at breakout that a fraction of the material at the progenitor surface gets accelerated to large velocities. In the sequence of models s11.3 to s11.8, we find increasing maximum ejecta speeds from 1800 km s^{-1} up to $\sim 13000 \text{ km s}^{-1}$, typically a factor of four higher than the mean mass-weighted velocity of the ejecta.

The general evolution of the long-term, post-breakout, photospheric conditions is qualitatively similar for this set of models. After breakout and for a few days, the internal energy stored in the shock-heated stellar envelope does work to accelerate the ejecta to its asymptotic velocity. For larger energy deposition, the expansion rate is greater and leads to more efficient cooling of the ejecta, thereby mitigating the impact of the larger internal energy initially provided by the shock. This cooling is quasi-adiabatic since little radiation is lost from the photon decoupling layers - it all occurs at large optical depth. After a few days, the ejecta velocity increases monotonically with radius (homologous expansion is only approx-

² Note that the shock is always supersonic and may propagate at very different speeds depending on location and initial energy deposition.

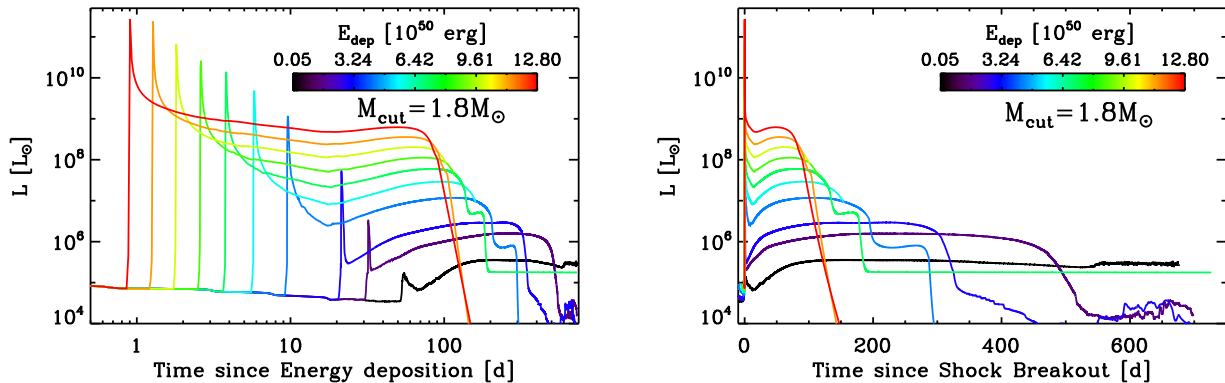


Figure 8. Same as Fig. 7, but this time showing the un-normalized bolometric luminosity. In the left panel, we use a logarithmic scale for the abscissa, showing the time since the start of the simulations. In the right panel, we use a linear scale for the abscissa, showing the time since shock breakout. Stronger explosions show shorter and stronger breakout signals, followed by a brighter plateau brightness but shorter plateau length. At intermediate values of the energy deposition, the plateau-brightness is followed by a ledge, which corresponds to the time when the photosphere recedes into the more tightly-bound (and slowly-expanding) helium-rich part of the envelope - no artificial nor physical mixing occurs in our 1D simulations, a process that could smear out such a feature. Note that for cases in which $E_{\text{dep}} \sim E_{\text{binding}}$, the breakout luminosity is barely larger than the following plateau, which we find here can last for up to two years in this $11 M_{\odot}$ progenitor star.

imately attained since the progenitor radius may represent up to 5–10% of the current photospheric radius at all times). As the ejecta expand, cool, and recombine to a lower ionization state, the photospheric velocity decreases with time. The photospheric radius first increases, reaching values in excess of 10^{15} cm for the high energy cases, but eventually decreases due to recombination and the diminishing optical depth of the ejecta. The location of the photosphere is that of full ionization, which for the H-rich composition of this stellar envelope occurs around 5000 K. Hence, the photospheric temperature, after its initial peak at breakout, slowly decreases to level off at ~ 5000 K. Ultimately, the photosphere reaches the inner region of the ejecta and the “event” enters its nebular phase. This transition occurs earlier for higher values of E_{dep} , after about 100 days in model s11.8 but up to ~ 200 days in the s11.3 model (since the code crashed for that model, this is an estimate based on the noticeable trend with energy deposition for that quantity; see Table 1).

This evolution in photospheric properties parallels the bolometric evolution of the explosion, which we show in Fig. 8. In all cases, the early breakout peak in luminosity is followed by a fading (initially from radiative cooling at the shock-heated surface layers) followed by a sustained brightness as the ejecta expand (the rate of increase in photospheric radius compensates the rate of decrease in photospheric temperature): This is the so-called plateau phase of Type II-P SNe. Peak luminosities, reached at a later time for a lower energy deposition (from 50 to 100 days after breakout), are in the range 3×10^7 up to $6 \times 10^8 L_{\odot}$. Similarly, the plateau duration lengthens with lower energy deposition, ranging from 100 up to about 200 days (recall that this occurs in models s11.3 to s11.8 for the same ejected mass of $\sim 8.8 M_{\odot}$). At the end of our simulations, we find time-integrated bolometric luminosities in the range 10^{48} – 10^{49} erg, which represent, in the same order, 1/20th down to 1/70th of the corresponding asymptotic ejecta kinetic energy.

Hence, at the high energy end, we obtain light curves that are reminiscent of Type II-P SNe (Fig. 1), ranging from the energetic events like SN 2006bp (Dessart et al. 2008), to the more standard SN 1999em (Leonard et al. 2002a), through to the low luminosity SN 1999br (Pastorello et al. 2009). The luminosity contrast of a factor of ~ 20 in this set of models is on the order of that inferred for

Type II-P SNe (Fig. 1; Pastorello et al. 2009). For moderate to high E_{dep} values, the plateau durations we obtain are on the order of those observed for Type II-P SNe, although we find a lengthening for lower E_{dep} values that has not been observed definitely. For example, the observations during the plateau phase of SN1999br are unfortunately truncated after 100 days, at a time when the SN was not showing a clear sign of fading. The subsequent observation 250 days later, when the SN has faded, does not exclude 99br kept its plateau brightness for a longer time, perhaps for a total of 150 or 200 days (see Fig. 1).

To summarize, the regime of explosions described in this section corresponds to that of type II-P SNe, with a range of explosion energies and bolometric luminosities that are in line with inferences from observations. The rather large energy-deposition magnitude (i.e. $\geq 4 \times 10^{49}$ erg) in this regime favors a scenario involving the gravitational collapse of the stellar core and, given the resulting complete envelope ejection, the formation of a neutron star remnant. We wish to emphasize that there is no fundamental limitation for preventing explosions in this $11 M_{\odot}$ model for energies as low as a few times 10^{49} erg, as in model s11.3. The corresponding light curve would be reminiscent of that of SN 1999br, only slightly fainter. We surmise such events do exist but may have been missed by current surveys, owing to the faint and slowly-evolving brightness of the event.

4.1.2 $E_{\text{dep}} \sim E_{\text{binding}}$

In this section, we continue the sequence toward lower energy deposition, entering a regime where its magnitude is on the order of the binding energy of the envelope, and, incidentally, on the same order as the total internal energy in the envelope. In contrast with results for high E_{dep} values, only a fraction of the progenitor envelope is ejected in models s11.01 to s11.2, ranging from 5.95 up to $8.6 M_{\odot}$. Despite the incomplete success for explosion, all models go through a similar sequence as that of powerful explosions. A shock crosses the progenitor envelope, heating it and propelling it outward. The shock eventually breaks out, after 10–30 d (time-average shock speeds of 150 – 500 km s^{-1}), with an ac-

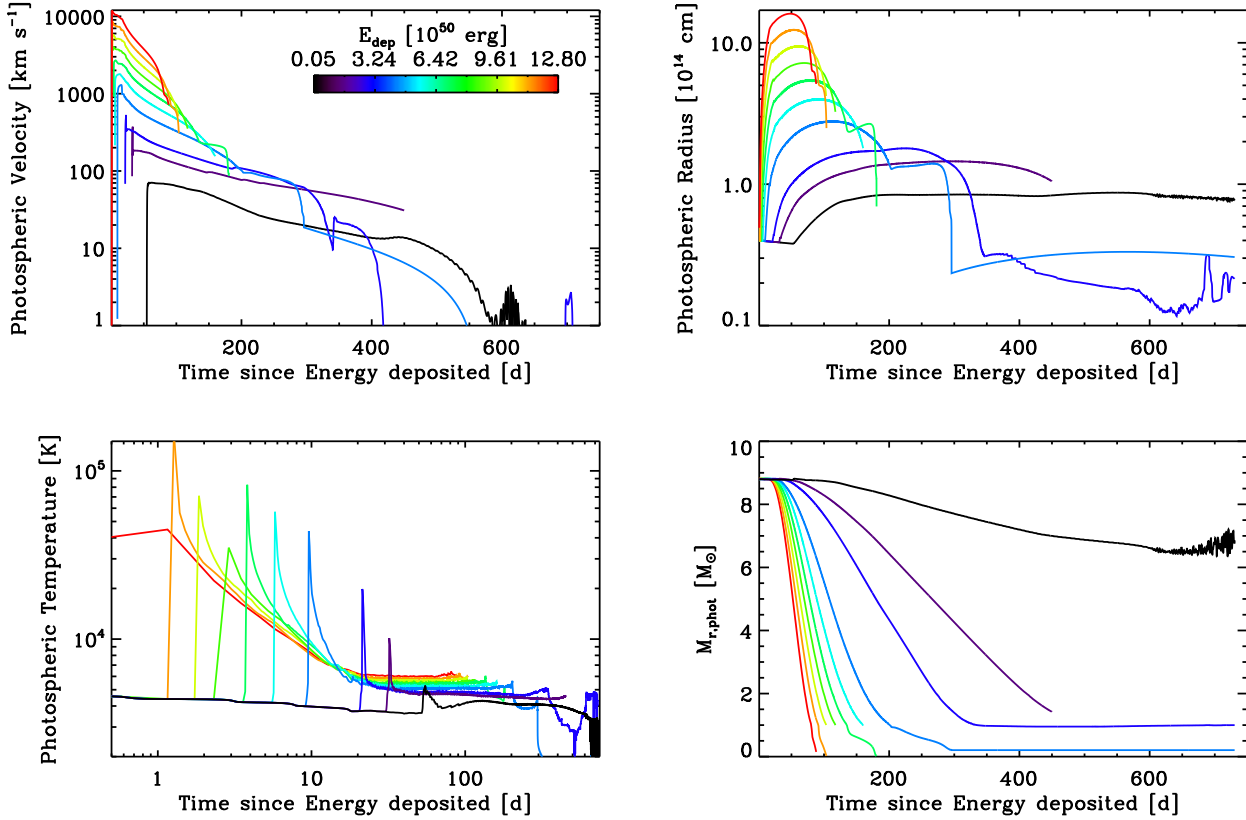


Figure 9. *Top left:* Time evolution of the velocity at the photosphere for the sequence of models associated with the $11 M_{\odot}$ model of WHW02. Only the energy deposited during the initial ten seconds after the start of the simulation differs between models, all initial model characteristics being the same. A color coding is used to distinguish the different cases, with total energy deposition encompassing the range 5×10^{48} (black) up to 1.28×10^{51} erg (red). *Top right:* Same as top left, but now for the radius at the photosphere. *Bottom left:* Same as top left, but now for the temperature at the photosphere. Note that the time of breakout is poorly sampled (dumps written every 10000 s), so that the temperature shown at breakout is an underestimate. *Bottom right:* Same as top left, but now showing the Lagrangian mass coordinate of the photosphere as a function of time. Note that the mass interior to the inner boundary of the V1D grid is $1.8 M_{\odot}$ for this sequence of models, and is not accounted for in this last panel.

companying peak luminosity of 3×10^6 up to $10^9 L_{\odot}$. The fastest ejected material is accelerated modestly, from 400 (s11_01 model) up to 1300 km s^{-1} (s11_2 model). At breakout, the kinetic energy of the envelope is a diminishing fraction of the total envelope energy, which is primarily stored internally. Asymptotically, the total kinetic energy of the material ejected (a fraction only of the total) is in the range 4×10^{47} up to 10^{49} erg, with mass-weighted average velocities in the range $70\text{--}300 \text{ km s}^{-1}$. The long-term light curves are characterized by peak luminosities in the range of $10^6\text{--}10^7 L_{\odot}$ and very long plateau durations of 1–2 years, yielding low-luminosity long-lived transients (Fig. 8). Hence, these events look somewhat like SNe because they attain luminosities/expansion-rates that are comparable to those of low-luminosity/energy Type II-P SNe. But they also look like giant eruptions as seen in the most massive luminous stars, characterized by super-Eddington luminosities on the order of $10^7 L_{\odot}$, with ejected shells weighing few solar masses and outflowing velocities of a few hundred km s^{-1} . The Eddington luminosity for this $10.6 M_{\odot}$ pre-SN star is $L_{\text{Edd}} = 4\pi cGM/\kappa \sim 4.07 \times 10^5 L_{\odot}$ (we use a representative mass-absorption coefficient $\kappa = 0.34 \text{ cm}^2 \text{ g}^{-1}$ for this hydrogen-rich stellar envelope), and hence, the luminosities quoted above in the range $10^6\text{--}10^7 L_{\odot}$ are all significantly super-Eddington. By contrast to radiative-driven outflows, the super-Eddington nature of the luminosity is only a

feature in the current context since the *ejecta* is already unbound after shock passage (this does not exclude secondary effects that could stem from the high luminosity).

The outcome of such a weak energy “explosion” can be two things. If the origin is a very weak energy release following core collapse, then the fraction of mass that was expelled will lead to a one-time transient, and the proto-neutron star will accumulate the inner part of the envelope, perhaps transitioning to a black hole if it becomes sufficiently massive (in the s11_01, it would form a black hole with a $3.85 M_{\odot}$ baryonic mass). But if the weak energy release is caused by something else, e.g. thermonuclear combustion of material at the surface of the degenerate (and hydrostatically-stable) core, the outcome is a massive eruption in a massive star. In this case, the luminosity eventually levels off, as the photosphere receding in mass through the ejecta layers eventually reaches the inner envelope layer that failed to eject. This second category of objects would be called SN impostors.³

³ In this case, the stellar core would eventually collapse, potentially ejecting the residual envelope, which is now of much lower mass and quasi hydrogen-deficient. Depending on the time delay between the two events, this could also produce a strong interaction with the previous ejected shell, yielding an interacting SN.

Unless the event occurs nearby and allows the inspection of the transient site, one does not know whether a star survived or not. Hence, such events are ambiguous and may be interpreted either as a one-time non-repeatable explosion (a SN) or a potential recidivist like η Car. These are impostors in the sense that they would not result from the collapse of a degenerate core, but they do share that important property with core-collapse SNe that, in the present context, they would result from shock-heating of the envelope. Hence, a breakout signal would systematically herald the forthcoming ejection, excluding its origin as a steady-state super-Eddington wind accelerated from a hydrostatic base. The longer duration of ~ 1 d and the softer distribution (UV-peaked) of the breakout signal should allow the detection of such events in large-scale sky surveys, providing a clear discriminant between an explosive or a steady-state-wind origin for such mass ejections.

4.1.3 $E_{\text{dep}} < E_{\text{binding}}$

For the smallest energy deposition value in our sequence (model s11_0; $E_{\text{dep}} = 5 \times 10^{48}$ erg), only a tiny fraction of the envelope ($\sim 0.13 M_{\odot}$) is ejected, concomitantly with shock breakout, while the bulk of the envelope remains attached to the star. The energy deposition is used to lift the envelope out of the gravitational potential well, but falling short from unbinding it. This results in a “bloated” star whose radius has increased by about a factor of two in 50 days after breakout, while the surface temperature has hardly changed. Consequently, the corresponding star, with its puffed-up envelope, brightens from a luminosity of $\sim 10^5 L_{\odot}$ up to $\sim 1.37 \times 10^5 L_{\odot}$, which remains well below its Eddington luminosity of $4.07 \times 10^5 L_{\odot}$.

Over the two-year timescale covered by the simulation, the photosphere retains a similar radius and temperature. Since the energy left over by the shock is stored at large optical depth, and since it was insufficient to communicate any kinetic energy to the envelope, the transport regime is no longer of dynamic diffusion (as in the high energy-deposition cases) but instead of static diffusion, with characteristic timescales of ~ 100 yr for this massive star envelope (Fig. 4). Albeit weak, such an energy deposition causes a significant translation of the star in the HR diagram and may be linked, in some cases, to the photometric and spectroscopic variability of H-rich massive stars. The central element that enables such low-energy perturbations to have any effect is the very low binding energy of massive star envelopes, in particular at the low-mass end.

4.2 Effect of varying the Energy-Deposition depth

We have argued in the introduction and in §2 that, physically, a deposition of energy from deep regions in the progenitor star is more likely since this is where most of the energy is stored or can be made available. This can occur through gravitational collapse of the degenerate core from its original radius of a few 1000 km to ~ 10 km (the standard initiation of a core-collapse SN explosion), or from violent shell burning above the core (our preferred trigger for transient phenomena in massive stars). In contrast, the envelope layers well above the core, characterized by lower densities and temperatures, tend to merely react to energy changes occurring at depth. It is, however, interesting to investigate the dependency of our results on the adopted site of energy deposition. We have thus performed two sequences for $E_{\text{dep}} = 10^{49}$ erg (model s11_1) and $E_{\text{dep}} = 4 \times 10^{49}$ erg (model s11_3), with a deposition at 1.8 (as

before), 3, 7, and 9 M_{\odot} Lagrangian mass coordinate. These correspond to locations in the helium or in the hydrogen shell. The deposition time in all cases is 10 s. We show the resulting light curves for both sequences in Fig. 10, with the corresponding key parameters given in Table 2.

For the s11_1 model sequence (black curve, left panel of Fig. 10), the energy deposition is on the order of the binding energy of the *entire* envelope above the $1.8 M_{\odot}$ mass cut. As we discussed before, this led to a SN-impostor-like event, with only a fraction of the total envelope ejected to infinity. The envelope outside of a $3 M_{\odot}$ mass cut has, however, only a 10^{47} erg binding energy so, as we move outward the site of energy deposition (from 3, to 7, and 9 M_{\odot} Lagrangian mass coordinate), we switch to a successful explosion with sizable kinetic energy and rapid light-curve evolution. As given in Table 2, the models with a mass cut at and beyond $3 M_{\odot}$ lead to full ejection of the layers exterior to the energy-deposition site, with representative ejecta expansion rates of $400\text{--}800 \text{ km s}^{-1}$ and kinetic energy of 10^{49} erg. Interestingly, the phase of high-brightness lasts from 90 up to 180 days despite the low amount of ejected material, i.e. between 1.6 and $7.6 M_{\odot}$. The long duration of these events, even for low ejected masses, is caused by two factors. First, the expansion is relatively slow so that radiative diffusion is modestly facilitated by the ejecta density reduction with time (we are closer to a static regime of radiative diffusion). Second, the energy losses through expansion are minimal since we start from a very extended (i.e. loosely-bound) stellar envelope. Note here that in the more compact (i.e. tightly-bound) progenitor configurations for Type I SNe (Wolf-Rayet stars or white dwarfs), the cooling through expansion is tremendous and the events owe their large brightness at a few weeks after explosion entirely to the heating caused by unstable isotopes with week-long half-lives. A corollary is that weak-energy ejections with little ^{56}Ni can only reach a large luminosity if they arise from a loosely-bound initial configuration, e.g. a big star.

For the s11_3 model sequence (light curve shown in the right panel of Fig. 10), the energy deposition is greater than the binding energy of the envelope above the $1.8 M_{\odot}$ mass cut so that no matter what the position of the mass cut is outside of $1.8 M_{\odot}$, we obtain full ejection of the shocked layers, with representative velocities in the range $500\text{--}1600 \text{ km s}^{-1}$.

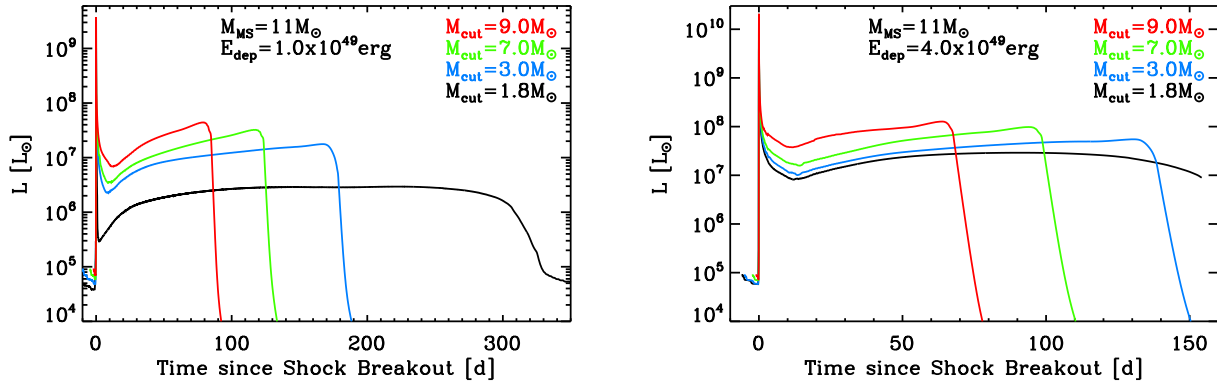
To conclude, we find that moving the energy-deposition mass cut M_{cut} outwards for a given energy-deposition magnitude E_{dep} produces a similar effect to increasing E_{dep} at a given M_{cut} . Quantitatively, this is modulated by the binding energy of the envelope exterior to M_{cut} . We observe in particular that it is possible to obtain light curves with a very extended plateau even for very small ejecta mass. Note that this remains an experiment though, since we believe the energy deposition in a massive star must occur in the vicinity of the core, hence interior to the Helium shell of pre-SN massive stars.

4.3 Effect of varying the Energy-Deposition duration

A fundamental element of our study is that energy deposition must occur on a short timescale to ensure the formation of a shock, rather than on a long time scale which would allow radiative diffusion and convection to carry outward the extra energy. In this section, we present results with VID for a model with $E_{\text{dep}} = 4 \times 10^{49}$ erg and $M_{\text{cut}} = 3 M_{\odot}$, but an energy-deposition time of 10 seconds, one hour, one day, one week, and one month. Since the resulting ejecta and bolometric properties are similar to those of the model s11_3-w3 (see Table 2), we do not tabulate the results for this se-

Table 2. Same as Table 1, but now showing the results for the sequence of models with differing energy deposition depth in the $11 M_{\odot}$ progenitor star (see §4.2 for discussion).

Model Name	s11_1	s11_1_w3	s11_1_w7	s11_1_w9	s11_3	s11_3_w3	s11_3_w7	s11_3_w9
E_{dep} (10^{50} erg)	1(-1)	1(-1)	1(-1)	1(-1)	4(-1)	4(-1)	4(-1)	4(-1)
M_{cut} (M_{\odot})	1.8	3.0	7.0	9.0	1.8	3.0	7.0	9.0
t_{dep} (s)	10	10	10	10	10	10	10	10
t_{end} (d)	730	450	450	354	160	200	200	200
M_{ejected} (M_{\odot})	7.75	7.60	3.60	1.60	8.72	7.60	3.60	1.60
$\langle v \rangle_M$ (km s^{-1})	121	350	520	804	510	715	1000	1600
$(E_{\text{kin}})_{\text{end}}$ (10^{50} erg)	1.3(-2)	1.0(-1)	1.0(-1)	1.0(-1)	2.8(-1)	4.1(-1)	4.1(-1)	4.3(-1)
$\langle v_{\text{max}} \rangle$ (km s^{-1})	560	1200	1430	1650	1800	2000	2400	3200
t_{SBO} (d)	21.4	9.7	4.3	1.8	5.8	5.0	2.2	0.9
$L_{\text{peak,SBO}}$ (L_{\odot})	5.2(7)	1.0(9)	1.8(9)	3.7(9)	4.9(9)	6.9(9)	1.2(10)	2.4(10)
$\langle v_{\text{shock}} \rangle$ (km s^{-1})	221	447	520	740	812	870	1000	1460
$(E_{\text{kin}})_{\text{SBO}}$ (erg)	6.7(47)	4.3(48)	3.3(48)	3.0(48)	1.3(49)	1.7(49)	1.3(49)	1.2(49)
$(E_{\text{int}})_{\text{SBO}}$ (erg)	3.8(48)	6.7(48)	7.6(48)	8.3(48)	1.7(49)	2.6(49)	3.0(49)	3.3(49)
$t_{\text{peak,plateau}}$ (d)	243	177	122	80	97	135	96	64
$L_{\text{peak,plateau}}$ (L_{\odot})	2.9(6)	1.8(7)	3.2(7)	4.4(7)	2.9(7)	5.4(7)	9.8(7)	1.3(8)
$\Delta t_{\text{plateau}}$ (d)	341	181	126	87	>155	142	102	71
$\int L_{\text{bol}} dt$ (10^{49} erg)	2.5(-2)	7.1(-2)	7.7(-2)	8.0(-2)	1.3(-1)	1.8(-1)	2.0(-1)	2.2(-1)

**Figure 10.** Same as Fig. 8 for the $11 M_{\odot}$ model, but now showing the emergent bolometric-light evolution resulting for cases in which the energy is deposited at a Lagrangian mass of 1.8 (black), 3 (blue), 7 (green), and $9 M_{\odot}$ (red). The left (right) panel corresponds to an energy deposition of 1 (4) $\times 10^{49}$ erg. In all cases, we choose the time origin as the time of shock breakout.

quence of models. However, we show the synthetic light curves in Fig. 11. In all cases, a phase of shock breakout takes place, followed by a bright plateau that persists over a similar duration. No qualitative difference is visible, and quantitative differences are small.

Hence, shock formation persists even for very long deposition times, despite the large range covered. In other words, a deposition of energy that takes place over a time scale much longer than the expected shock revival time in core-collapse SN explosion (i.e. one second) still leads to shock formation. We are aware that the neglect of feedback effects makes this exploration somewhat artificial. In the context of a nuclear flash, expansion could, for example, endanger the continuation of nuclear burning.

For energy deposition timescales much longer than a month, a diffusion wave, rather than a shock, would form, together perhaps with convection. Such a regime, not of interest in the present study, would have to be followed in 2D or 3D (see, for example, Mocák et al. 2008, 2009) to properly model the interplay between these two means of energy transport and the resulting effects on the envelope structure.

4.4 Dependency on Progenitor Mass

The choice of the $11 M_{\odot}$ model for the investigations presented so far was motivated by the lower density of the progenitor envelope. This produces larger Courant-time increments for the hydrodynamics and easier computing. However, as evidenced by the variation in envelope binding energy for 10 – $40 M_{\odot}$ massive stars (recall that these model masses correspond to those on the main sequence; the corresponding masses at the onset of collapse can be seen from Fig. 2) and by the dependencies presented in the previous sections, a given energy deposition will obviously produce a very different outcome for different progenitor masses. In this section, we thus explore the radiative and dynamical properties of ejecta produced by the deposition of 10^{50} erg at the base of the helium shell in 11 , 15 , 20 , and $25 M_{\odot}$ massive-star progenitors. In the same order, this corresponds to mass cuts at 1.8 , 3.1 , 5.0 , and $7.2 M_{\odot}$ in the envelope, to envelope binding energies (we quote absolute values) of 9.9×10^{48} erg, 4.6×10^{49} erg, 6.6×10^{49} erg, and 1.4×10^{50} erg, and to total progenitor masses at the time of collapse of 10.6 , 12.6 , 14.7 , and $12.5 M_{\odot}$. We show the resulting light curves in Fig. 12.

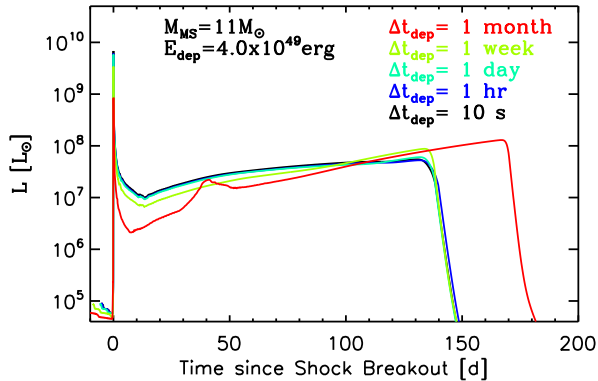


Figure 11. Same as Fig. 8, but now showing the bolometric light evolution resulting from models in which the energy is deposited at a fixed rate over 10 s (black), 1 hr (blue), 1 d (light green), 1 week (green), and 1 month (red). The site of energy deposition is at Lagrangian-mass coordinate $3 M_\odot$ and the energy deposition is 4×10^{49} erg in all cases. The time origin is the time of shock breakout.

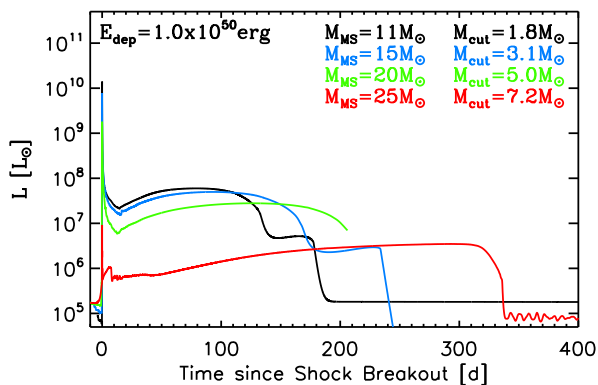


Figure 12. Same as Fig. 8, but now showing the bolometric light evolution for different progenitor-mass models: 11 (black), 15 (blue), 20 (green), and 25 M_\odot (red; these masses correspond to main-sequence masses). In all models, we deposit the same energy of 10^{50} erg, and at the same *physical* location in the envelope, corresponding to the base of the helium shell. In the same order, this corresponds to the Lagrangian-mass coordinate of 1.8, 3.1, 5.0, and 7.2 M_\odot . The time origin is the time of shock breakout, which corresponds to a range of delays since energy-deposition in the four models.

As before with the exploration of outcomes for varying energy-deposition magnitudes (§4.1) or sites (§4.2), adopting different progenitor stars and depositing the energy in regions that are more or less bound leads to a similar modulation in light-curve properties. With the adopted value $E_{\text{dep}} = 10^{50}$ erg, we obtain light curves reminiscent of low-luminosity Type II-P SNe if it is larger than the binding energy of the overlying envelope (11 and 15 M_\odot models), and long-lived and fainter events reminiscent of SN impostors or low-energy transients otherwise (20 and 25 M_\odot models).

Note that if, using the same progenitors (11, 15, 20, and 25 M_\odot main-sequence mass models), we deposit a given energy at a radius where the Lagrangian mass is $2 M_\odot$ lower than the total progenitor mass (same shell mass underneath the progeni-

tor surface), we obtain essentially the same light curves and ejecta properties for all models. This degeneracy results from the generic $\sim 10^{47}$ erg binding energy of the corresponding (outer) H-rich shell in these different stars.

To summarize, and perhaps paradoxically, the consideration of these additional progenitors (with different envelope structure/binding energy) does not add any new perspective to our results so far since the diversity of outcomes was fully revealed earlier on with the 11 M_\odot model through the variation of the values of E_{dep} and M_{cut} .

5 SAMPLE OF NON-LTE SYNTHETIC SPECTRA AT 5 DAYS AFTER SHOCK BREAKOUT

In this section, we provide synthetic spectra that illustrate the spectral-energy distribution of the various models discussed above. We choose the representative time of five days after shock breakout since it is a typical discovery time for SNe, and perhaps as well for optical transients etc. This also offers a unique reference time for comparison in all models. We focus on the models presented in §4.1 in which only the energy deposition magnitude is varied, using the 11 M_\odot model and adopting a deposition site at the 1.8 M_\odot Lagrangian-mass coordinate.

The computation we perform follows the approach described in various contexts in Dessart & Hillier (2006); Dessart et al. (2008, 2009). Using the results from our V1D computations, we extract the gas properties at a total optical depth of a few tens and at a time of about five days after shock breakout. We then use these characteristics of radius, density, temperature, and velocity (see Fig. 9) to setup the initial conditions for the non-LTE radiative-transfer calculation. At such early times, the photosphere resides in the outer hydrogen-rich part of the progenitor envelope, characterized by a typical RSG surface composition (see, e.g., Dessart et al. 2008). We adopt a density exponent of ten and a homologous expansion. Recall that the line and continuum formation regions are rather confined and hence such characteristics, in practice, really matter *locally*, i.e. the density/velocity distributions may vary differently in a global sense (for details, see Dessart et al. 2009). We show in Fig. 13 the synthetic spectra (i.e. the emergent flux in the observer's frame), assuming a distance of 10 Mpc and neglecting any reddening.

At that reference time, and from the high to the low energy-deposition case, we obtain a trend towards smaller ejecta velocity (narrower line profiles), smaller temperature (redder peak flux distribution), combined with a smaller radius (smaller flux). At higher energy deposition, the synthetic spectra are reminiscent of Type II-P SNe (from standard to low-luminosity ones), while for lower energy deposition, the spectra are qualitatively similar to those of cool mass-losing stars like the present day η Car or SN impostors like SN 2002kg (Maund et al. 2006). We thus recover spectroscopically the various regimes identified in bolometric light curves and ejecta properties, primarily through modulations in luminosity and line width. An interesting aspect of this set of simulations is that for H-rich massive stars (and as long as the temperatures are not too low to foster the formation of molecules and dust), we obtain a very uniform set of spectral features (with the dominance of hydrogen and metals, whose abundance is that of the environment in which the star was born), merely varying in widths, with slight changes in the flux distribution mostly associated with variations in ionization. For example, the LBV η Car has the same surface composition as the progenitor of SN 1999em (Hillier et al. 2001; Dessart & Hillier

2006); it also has similar line-profile morphology and flux distribution as that of the interacting SN 1994W (Dessart et al. 2009). This spectroscopic uniformity adds to the difficulty of inferring the dynamical origin of the event.

6 DISCUSSION

In this section, we discuss the ramifications of our results for explosions and eruptions in massive stars. Let us stress again that we do not make the claim that all massive-star mass ejections, or all transients in general, stem from a strong, sudden, and deeply-rooted energy release in the progenitor-star envelope. But here, given this working hypothesis, we explore its potential for explaining the properties and the diversity of observed transient phenomena associated with massive stars.

6.1 Binding energy considerations

The binding energy is the most fundamental quantity controlling the outcome of a given energy deposition. Although this conclusion seems trivial, its implications are far-reaching.

Since the binding energy of massive stars increases with progenitor mass, SN explosions arising from more massive progenitors will, on average, be more energetic. Indeed, the energy deposition at the base of the envelope to be ejected has to be a few units of the binding energy, one unit to unbind the envelope, and the remaining units to give it its kinetic energy (fast expansion) and internal energy (bright display). In the sample of massive stars studied here, the envelope binding energy (right panel of Fig. 3) sets a higher energy threshold for increasing progenitor main-sequence mass. Consequently, stars originally more massive than $\sim 15 M_{\odot}$ require an energy deposition of at least 10^{51} erg to unbind the envelope while 100 times less is sufficient in a $10 M_{\odot}$ progenitor. We surmise that in our sample, low-energy explosions will naturally be associated with the least-bound objects, i.e. the low-mass massive stars. We can illustrate our argument with the following example: for a low-energy, e.g. 10^{49} erg, transient to be associated with a $15 M_{\odot}$ progenitor star requires an energy deposition of merely 1% greater than the binding energy. This excess energy is so small compared to the binding energy of the envelope that the required tuning to make this low-energy ejection can hardly be met. Hence, low-energy transients associated with stars should stem from ejection of loosely-bound regions, for example the envelope of low-mass massive stars or, in another context, low-mass shells at the surface of a white dwarf. Obviously, this is relevant only if any such energy deposition can take place but observations of transients demonstrate that it can. How it does it is a question left for future work.

As more and more energy is needed to eject the envelopes of more massive progenitors, the extreme case of tightly bound Wolf-Rayet stars can only be associated with very energetic explosions. The fact that (nearly) all hypernovae are associated with Type Ib/c SNe is in this respect quite compelling. It is not so much that they somehow can achieve higher energy deposition; it is that they *must* (the fact that they do achieve a higher energy-deposition to explode is an interesting problem that concerns the explosion mechanism, neutrino physics, magneto-rotational effects etc). In other words, of all possible scenarios, *only* those that lead to a very large energy deposition (well in excess of the binding energy) can yield a successful, and visible, explosion. This may act as a natural tuning ingredient to favor fast-rotating cores in tightly-bound progenitors

like Wolf-Rayet stars (Burrows et al. 2007a). The fraction of Wolf-Rayet stars that fail to explode following core collapse is unknown at present.

This binding-energy argument may also be a very natural explanation for the lack of detection of Type II SN explosions for objects with main sequence mass greater than $\sim 20 M_{\odot}$ (Smartt 2009). The standard neutrino mechanism may, after all, fail to deliver an energy that is comparable to the binding energy of the more massive progenitor stars. And indeed, this may not be so surprising given the ten order of magnitude density contrast in the region $2-5 M_{\odot}$ between the 11 and the $25 M_{\odot}$ models of WHW02 (Fig. 2). This would suggest that a lot of core-collapse events associated with the higher mass massive stars do not yield explosions, but instead form a black hole with no transient electromagnetic display (see Smartt 2009). The proposition of Kochanek et al. (2008) to monitor a large number of red supergiants for failed explosion would nourish this option.

It is the low binding energy (hence extended envelope structure) of massive stars that causes the bright displays of their ejected envelopes, even for low energy deposition, and even in the absence of any heating from unstable isotopes. In general, the change from a modest-size progenitor star to an extended ejecta causes a dramatic cooling, primarily due to expansion. And indeed, in Type Ia/b/c SNe, this cooling is dramatic and the large SN luminosity results only because of the presence of unstable isotopes, whose half-life of days to weeks makes the SN bright on a comparable timescale. In contrast, only modest radial expansion (typically by 2 orders of magnitude compared to 5–7 in Type I SNe) occurs after the explosion of the already extended envelopes of massive stars. In such objects, large luminosities of $10^7-10^8 L_{\odot}$ can be achieved without the contribution from unstable isotopes, and even for modest ejecta kinetic energies.

Hence, in general, low-energy (stellar) explosions/eruptions should occur from regions that are weakly gravitationally-bound. Given the very low envelope binding energy of low-mass massive stars and hence the very low energy threshold for producing explosion/eruption, we argue that these should be prime candidates for transient events in the Universe, perhaps even in connection to interacting SNe. The stellar initial-mass function is also biased in favor of such low-mass massive stars, which are therefore not rare (about one for every 200 solar-type stars). This argumentation likely applies to SN 2008S (Prieto et al. 2008; Smith et al. 2009a; Botticella et al. 2009), M85-OT2006-1 (Kulkarni et al. 2007; Pastorello et al. 2007), or the enigmatic SN2008ha (Foley et al. 2009; Valenti et al. 2009). For the latter, the association of the low-energy low-luminosity ejecta with a Wolf-Rayet progenitor, a highly-bound object, seems unlikely.

6.2 Explosion/eruption associated with transient phenomena

A growing sample of transient objects possess intermediate luminosities between SNe and novae. Their origin is debated. Owing to their low energy, the community has argued for either a weak-energy core-collapse SN explosion (e.g. Botticella et al. 2009; Pastorello et al. 2009), or for a super-Eddington wind in a SN impostor (e.g. Maund et al. 2006; Smith et al. 2009b). The ambiguity stems from the common energy-ground in which events associated with these two scenarios fall, the $\lesssim 10^{50}$ erg kinetic energy of the homunculus associated with η Car rivaling that of low-luminosity Type II-P SNe. Reversing the argument, how many of these low-luminosity Type II-P SNe are in fact impostors, boasting ejecta kinetic energy that are well below that of LBVs? The “SN”

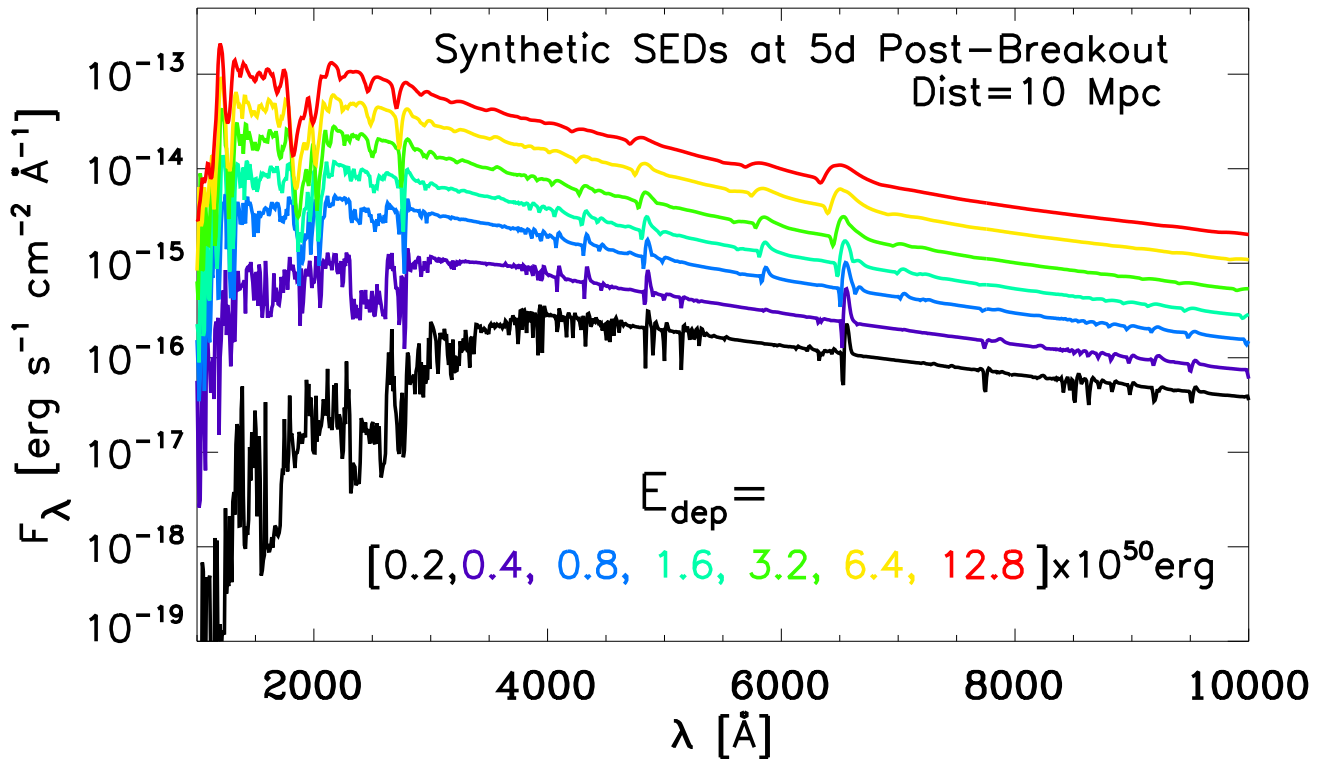


Figure 13. Non-LTE synthetic spectra for the models presented in §4.1, based on the ejecta properties computed with V1D and extracted at a representative time of 5 days after shock breakout (we scale the synthetic fluxes adopting a distance to the object of 10 Mpc). Notice how, despite the 2-order-of-magnitude range in energy deposition in this model sequence, the resulting spectral-energy distributions are qualitatively similar, differing essentially in the absolute flux level (the larger the energy deposition, the more luminous the event) and in line-profile width (the larger the energy deposition, the larger the ejecta kinetic energy). This similarity is also seen in observations of hydrogen-rich transients and results from the comparable envelope composition of the progenitor star and the comparable ionization state at the ejecta at the photosphere.

status in this energy regime seems to be often based on faith rather than unambiguous observational or theoretical evidence.

In the shock-heated solutions we presented in §4.1, the ejecta are systematically turned into a radiation-dominated plasma. At shock breakout, they are essentially unbound (their total energy $E_{\text{grav}} + E_{\text{kin}} + E_{\text{int}}$ is positive) and possess a large amount of internal energy. In those models with low-expansion velocity and super-Eddington luminosities of 10^6 – $10^7 L_{\odot}$, the photosphere has properties that are comparable to those of erupting LBVs, yet their super-Eddington luminosity plays no role in driving the material, which was already unbound after shock passage. From an inspection of the long-term light curve, it seems difficult to distinguish between the two since the timescale over which the radiative display evolves is very long and related to radiative diffusion: Apart from the breakout signature, it bears no imprint of the explosive origin, i.e. the sudden and deeply-rooted release of energy.

The recent observation of fast-moving material ahead of η Car’s homunculus points very strongly toward a shock-heated envelope as the origin of the giant eruption (Smith 2008). The invocation of a super-Eddington wind in the low-mass progenitor star associated with SN2008S may be supporting the same hypothesis since low-mass massive stars are well below their Eddington limit, while a shock could easily take them beyond that limit. An interesting and generic component of all the shock-heating scenarios

that we explored in this paper is the associated shock-breakout signal, whose detection could therefore disentangle situations associated with a quasi-steady wind from a hydrostatically-bound super-Eddington atmosphere on the one hand from those associated with a slowly-moving shock-heated ejecta on the other hand.

6.3 Variability in Massive stars

While the binding energy of massive star envelopes increases with progenitor mass, the mean binding energy is low for all objects that have retained a hydrogen envelope. In particular, and in the models of WHW02, that outer H-rich shell has a very uniform and very low binding energy of 10^{47} erg. Owing to mass loss, the mass of that shell decreases with time for higher-mass massive stars, but it always remains loosely bound. In our simulations, we found that even for a very modest energy deposition, well below the binding-energy value, important structural changes of the envelope occurred.

We suspect that hydrodynamic-fluid instabilities taking place deep in the stellar interior (Bazan & Arnett 1994, 1998; Asida & Arnett 2000; Arnett et al. 2005; Meakin & Arnett 2006) may provide the energy seed for at least a fraction of the variability observed in massive stars. This has not been fully realized so far in part because studies of stellar variability tend to isolate the surface layers and ignore the interior, while studies of stellar interi-

ors reduce all the complicated physics occurring near the surface to imposed and simplified conditions at the grid outer boundary (see, however, Cantiello et al. 2009). We expect that, owing to their huge surface radii and therefore low binding energy, supergiant and hypergiant stars should be very sensitive to such perturbations from the stellar interior, and indeed observations of such stars reveal a rich and violent mass-loss history (Smith et al. 2009b). Similarly, objects that through the course of their *quasi-steady* evolution happen to lie close to the Eddington limit and/or reach critical rotation are naturally more exposed to potential *time-dependent* deeply-rooted energy leaks.

This does not exclude the role of other mechanisms for mass ejections, for example, pulsations, rotation, radiation-driven mass loss etc., although it is at present not clear how these processes can produce the extreme properties required in the context of high-luminosity interacting SNe or giant eruptions of LBVs.

7 CONCLUSIONS

In this paper, we have presented one-dimensional one-group (gray) two-temperature radiation-hydrodynamics simulations of pre-SN massive-star envelopes subject to a sudden release of energy above their degenerate core. Although at the high energy end, the likely phenomenon is core collapse, we more generally have in mind the thermonuclear incineration of intermediate-mass elements present in shells above the core. The motivation for this study is: 1) The existence of interacting SNe (which must eject a shell at least once before core-collapse, but more likely eject multiple shells, by some means not elucidated so far); 2) the identification of fast-moving material exterior to η Car's homunculus (which cannot stem from radiation-driving in a wind; Smith 2008); 3) the broad range of energies inferred for Type II-P SNe, overlapping at the low-energy end with high-energy transients and massive-star eruptions. The bulk of our results stem from work on the $11 M_{\odot}$ model of WHW02, although tests with higher-mass progenitors yield the same qualitative conclusions and regimes, merely shifted quantitatively. This work is an exploration of the outcome of a strong, sudden, and deeply-rooted energy deposition taking place at the base of a massive-star envelope. We are not proposing this scenario holds for all massive-star mass ejections, but we investigate what results when this circumstance obtains. There is no doubt it does, but how frequently and how robustly is left for future study.

Although this result is not new, we find that the fundamental quantity controlling the outcome of a strong, sudden, and deeply-rooted energy deposition is the binding energy of the stellar envelope, which increases considerably with progenitor mass in the range $10\text{--}40 M_{\odot}$. What is new, however, is our study of the long-term evolution of the gas and radiative properties that result from configurations where the energy deposited is greater, on the order of, or less than the envelope binding energy. We identify three regimes, with a continuous progression from 1) SN explosions at high energy ($E_{\text{dep}} > E_{\text{binding}}$), with a complete envelope ejection associated with a 100-day long high-plateau luminosity; 2) SN impostors at the intermediate energy range ($E_{\text{dep}} \sim E_{\text{binding}}$), with a partial envelope ejection, and a more modest but longer-lived plateau luminosity; and 3) bloated/variable stars at the low-energy end ($E_{\text{dep}} < E_{\text{binding}}$), with little or no mass ejection but with a residual puffed-up envelope of weakly-modified properties. What conditions the results is not the magnitude of the energy deposition itself but how it compares with the binding energy of the envelope exterior to the site of deposition. Hence, to achieve the same re-

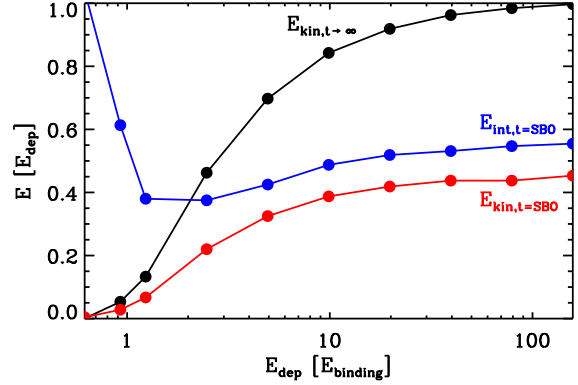


Figure 14. Correlation between various energies (normalized to the corresponding adopted energy deposition) and the energy deposition (normalized to the corresponding envelope binding energy). In black, we show the normalized asymptotic energy of the ejecta/outflow, and in blue (red) the normalized envelope/ejecta internal (kinetic) energy at the time of shock breakout. Only the models presented in Table 1 are shown here. The black curve illustrates the three regimes we have presented here, with SN explosions, SN impostors, and variable/perturbed stars as the energy deposition varies from being much larger, comparable, and smaller than the envelope binding energy. Notice how the internal energy always dominates over the kinetic energy at the time of shock breakout in the simulations performed here.

sult requires more energy in a more massive progenitor star. These properties are summarized in Fig. 14.

In all simulations presented, a shock forms systematically with a strength that depends on the energy deposited. It crosses the envelope in ~ 1 to ~ 50 days, hence communicating its energy to the entire progenitor envelope *quasi-instantaneously*, i.e. as opposed to, e.g., a diffusion timescale for energy transport of 10^4 years or more at the corresponding depth. This shock eventually emerges at the progenitor surface with a breakout signal that varies from a duration of an hour up to a few days (modulated here by the shock speed rather than by the atmospheric-scale height), with a flux peaking at longer wavelengths for weaker shock strengths. This breakout signal is the (and may be the only) *unambiguous* evidence that the subsequent “ejection” was triggered by shock-heating, and thus has an explosive origin.

At shock breakout, the luminosity reaches a peak, then fades, before stabilizing/rising again forming an extended plateau. This plateau phase corresponds to the recombination epoch of the ejected mass, the internal energy decreasing primarily through expansion and little through radiation. It is the large stored internal energy (in the form of radiation) that keeps the ejecta optically thick and luminous (radioactive decay is neglected in our work). We find a continuum of light curves, faster-expanding ejecta being more luminous both at breakout (stronger shock) and during the plateau phase (Fig. 15). The models presented in §4.1 corroborate the correlation between plateau luminosity and mid-plateau photospheric velocity identified by Hamuy & Pinto (2002), and refined by Nugent et al. (2006); Poznanski et al. (2009). We also find that the plateau duration is anti-correlated with energy deposition (Fig. 16). At larger energy, faster expansion leads to faster cooling and recombination so that the ejecta photosphere recedes faster in mass/radius after reaching its peak earlier. For small energy variations in this regime, interplay between kinetic and internal energy (which are comparable at breakout) yield a plateau duration

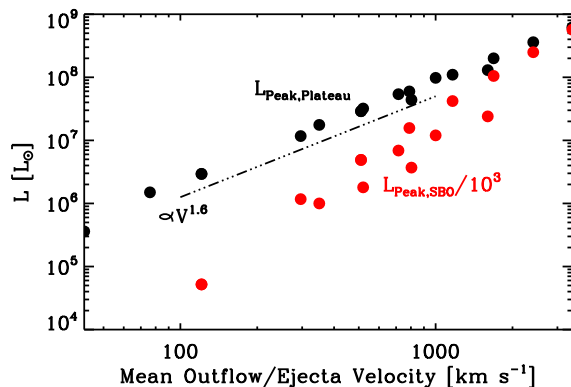


Figure 15. Correlation between the peak luminosity during the plateau phase (black dots) and the mass-weighted average ejecta velocity. We also show the correlation for the peak luminosity at shock breakout (red dots; scaled down by a factor of 1000 for convenience). Note that we include models from Tables 1 and 2. We overplot the line $L \propto v^{1.6}$, which follows closely the distribution of points for $L_{\text{Peak,Plateau}}$ versus $\langle v \rangle_M$. Our radiation-hydrodynamics simulations support the correlation identified by Hamuy & Pinto (2002) and subsequently improved upon by Nugent et al. (2006); Poznanski et al. (2009). Our slope is in close agreement with that proposed in this last reference. Impressively, the relation holds over the entire domain explored. Note that there is no consideration of radioactive decay from unstable isotopes or departures from spherical symmetry, and only data points associated with the $11 M_{\odot}$ -progenitor star are used. Relaxing these choices would likely introduce some scatter.

that is ~ 100 d, which is on the order of Type II-P plateau lengths. For lower energy deposition, we switch slowly from a regime of dynamic diffusion to that of quasi-static diffusion. The more slowly-expanding ejecta, characterized by a slowly-decreasing optical depth with time, gives the bolometric luminosity a modest peak value and a slow evolution, with plateau durations of up to 1-2 years. The plateau phase is thus more extended and fainter for lower energy deposition, echoing the light-curve trend going from SNe to SN impostors (Fig. 1). Note that, in our simulations, these timescales are always 6-7 orders of magnitude larger than the timescale for the energy deposition, which was chosen to be ten seconds in most cases. In other words, the timescale over which the light curve evolves (basically that of radiative diffusion in an expanding medium) has no connection to the timescale over which the energy was deposited in the first place.

From our exploration and with our set of models, we find that explosions of varying strength can yield the broadest range of outcomes in *low-mass* massive stars because they are characterized by a very low envelope binding energy (Fig. 3). We indeed obtain light curves evolving from week to year timescales (Fig. 8) and ejecta expansion rates ranging from a few tens to a few thousand km s^{-1} (Fig. 9). An explosion/eruption producing a transient requires merely 10^{49} erg in such objects, a value that is so low that gravitational collapse of the stellar core may not be required. And indeed, in this mass range, stellar-evolutionary calculations reveal the existence of nuclear flashes in the last nuclear-burning stages (Weaver & Woosley 1979), which could represent such an energy source. We therefore propose that low-mass massive stars are prime candidates for transient phenomena in the Universe, as well as prime candidates for interacting SNe such as 1994W (Dessart et al. 2009).

In our simulations, sudden energy deposition above the core

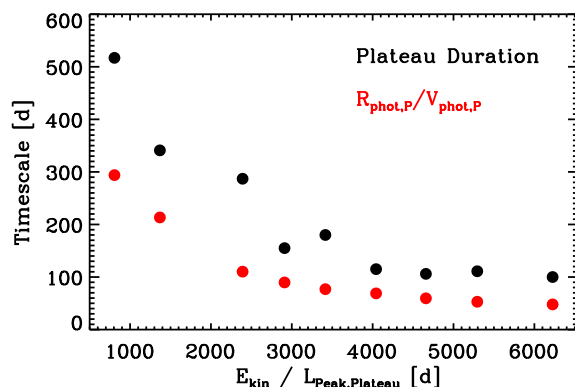


Figure 16. Correlation between the plateau duration (black) and the time-like quantity $R_{\text{phot,P}}/V_{\text{phot,P}}$ (ratio of the radius and the velocity at the photosphere at the time of peak-plateau brightness) versus the time-like quantity equal to the asymptotic ejecta kinetic energy divided by the peak-plateau luminosity brightness.

leads to shock-heating of the *entire* envelope. Whenever the energy deposited is greater than its binding energy, the *entire* envelope is ejected, with an asymptotic kinetic energy that is commensurate with the energy deposited. If a subsequent energy deposition occurs (e.g. a nuclear flash followed by gravitational collapse, as needed in a fraction at least of interacting SNe), the second ejection would have low mass and little or no hydrogen. Depending on the time between the two ejections, one could get an interacting SN for a short delay (i.e. a few years) or two transients at the same location for a long delay (the first one being dim if the explosion energy is small and the second one being potentially very dim due to the low ejected mass). These scenarios are rather speculative, but they are warranted since at present most, if not all, transients have an unknown origin and are poorly characterized.

In our simulations, and within the context of this work, we obtain small mass ejections only when depositing the energy close to the progenitor surface, an eventuality that seems difficult to justify physically in such massive stars. Such low-mass ejections would seem to be better suited, for example, to the surface layers of an extended white dwarf.

Synthetic spectra computed for a sequence of models with varying energy deposition reveal a continuous evolution from Type II-P SN-like spectra at high energy ($L \sim 10^8 L_{\odot}$), to low-luminosity Type II-P SN spectra at intermediate energy ($L \sim 10^7 L_{\odot}$), to SN-impostor-like spectra at low energy ($L \sim 10^6 L_{\odot}$), with, in the same order, narrower line profiles and redder/cooler spectral-energy distributions (Fig. 13).

The results from this work should not be compromised by the approximations made in our radiation-hydrodynamics simulations. First, with one dimensionality we prevent convective transport and any structure formation through, e.g., Rayleigh-Taylor instabilities. This may alter the properties of models characterized by low expansion speeds (longer evolution timescale); we thus plan to study this eventuality with 2D and 3D simulations in the future. Second, we deposit the energy at a large and fixed rate, independent of any feedback effects. In the case of nuclear flashes, such feedback effects could shut-off the burning prematurely. We are aware of this artifact and will attempt in future work to develop a more physically-consistent approach by investigating the conditions that may lead to shock formation, rather than assuming a setup that systemati-

cally leads to it. However, provided a shock forms, we think our results apply. Third, progenitor models may differ on a mass-by-mass comparison with other groups but the general trend of increasing binding energy with main sequence mass should hold. Fourth, one-group transport should be accurate enough since it has been shown to capture the essentials of such radiation hydrodynamics simulations (Utrobin & Chugai 2009) - the key physics presented here takes place at large optical depth, under LTE conditions.

Our finding that very modest energy perturbations can dramatically affect the structure of a massive star motivates detailed multi-dimensional hydrodynamical investigations of massive-star interiors, in particular of the last burning stages preceding core-collapse (see, e.g., Bazan & Arnett 1994, 1998; Asida & Arnett 2000; Arnett et al. 2005; Meakin & Arnett 2006). As shown in these hydrodynamical simulations, and more generally, we surmise that the quasi-steady state approach of standard stellar-evolutionary codes (which keep an eye on the longer-term evolution of stars) may be missing important ingredients for our understanding of massive-star evolution. This has relevance for understanding mass loss and in particular massive-star eruptions, stellar variability/stability, and interacting SNe. Such pre-SN mass ejections would also modify, and perhaps sizably, the envelope mass and structure, thereby affecting the conditions surrounding core collapse and explosion.

Ongoing and forthcoming surveys/missions like Pan-STARRS, Sky Mapper, the Palomar Transient Factory, GALEX, or the Large Synoptic Survey Telescope will better reveal the diversity of explosions, eruptions, and more generally transient phenomena in the Universe. We surmise that surveys up to now have missed a large number of low-energy long-lived transients, such as low-luminosity Type II-P SNe (objects even less energetic than SN1999br) and SN impostors. It is somewhat surprising that we have not yet detected Type II SNe with Plateau durations well in excess of 100 days. Moreover, for the shock-heating solutions presented here, a breakout signal systematically takes place. At SN-like energies, the signal may be too short to be resolved (Gezari et al. 2008), but for lower-energy transients, the reduced shock speed and strength would lengthen the breakout duration up to about a day, and move the peak of the spectral-energy distribution from $\sim 100\text{\AA}$ to the 1000-3000 \AA range. Hence, the breakout signal should be more easily detectable in such transients, allowing to distinguish between an explosive event and, e.g., a super-Eddington wind.

REFERENCES

- Arnett, D., Meakin, C., & Young, P. A. 2005, in *Astronomical Society of the Pacific Conference Series*, Vol. 332, *The Fate of the Most Massive Stars*, ed. R. Humphreys & K. Stanek, 75–
Asida, S. M. & Arnett, D. 2000, *ApJ*, 545, 435
Bazan, G. & Arnett, D. 1994, *ApJL*, 433, L41
—. 1998, *ApJ*, 496, 316
Blinnikov, S., Lundqvist, P., Bartunov, O., Nomoto, K., & Iwamoto, K. 2000, *ApJ*, 532, 1132
Botticella, M. T., Pastorello, A., Smartt, S. J., Meikle, W. P. S., Benetti, S., Kotak, R., Cappellaro, E., Crockett, R. M., Mattila, S., Sereno, M., Patat, F., Tsvetkov, D., van Loon, J. T., Abraham, D., Agnoletto, I., Arbour, R., Benn, C., di Rico, G., Elias-Rosa, N., Gorshonov, D. L., Harutyunyan, A., Hunter, D., Lorenzi, V., Keenan, F. P., Maguire, K., Mendez, J., Mobberley, M., Navasardyan, H., Ries, C., Stanishev, V., Taubenberger, S., Trundle, C., Turatto, M., & Volkov, I. M. 2009, *MNRAS*, 398, 1041
Burrows, A., Dessart, L., Livne, E., Ott, C. D., & Murphy, J. 2007a, *ApJ*, 664, 416
Burrows, A. & Goshy, J. 1993, *ApJL*, 416, L75+
Burrows, A., Livne, E., Dessart, L., Ott, C. D., & Murphy, J. 2007b, *ApJ*, 655, 416
Cantiello, M., Langer, N., Brott, I., de Koter, A., Shore, S. N., Vink, J. S., Voegler, A., Lennon, D. J., & Yoon, S.-C. 2009, *A&A*, 499, 279
Chugai, N. N. & Utrobin, V. P. 2000, *A&A*, 354, 557
Dessart, L., Blondin, S., Brown, P. J., Hicken, M., Hillier, D. J., Holland, S. T., Immler, S., Kirshner, R. P., Milne, P., Modjaz, M., & Roming, P. W. A. 2008, *ApJ*, 675, 644
Dessart, L. & Hillier, D. J. 2005a, *A&A*, 439, 671
—. 2005b, *A&A*, 437, 667
—. 2006, *A&A*, 447, 691
Dessart, L., Hillier, D. J., Gezari, S., Basa, S., & Matheson, T. 2009, *MNRAS*, 394, 21
Drissen, L., Crowther, P. A., Smith, L. J., Robert, C., Roy, J.-R., & Hillier, D. J. 2001, *ApJ*, 546, 484
Ensman, L. 1994, *ApJ*, 424, 275
Ensman, L. M. 1991, PhD thesis, AA(California Univ., Santa Cruz.)
Falk, S. W. & Arnett, W. D. 1977, *ApJS*, 33, 515
Foley, R. J., Chornock, R., Filippenko, A. V., Ganeshalingam, M., Kirshner, R. P., Li, W., Cenko, S. B., Challis, P. J., Friedman, A. S., Modjaz, M., Silverman, J. M., & Wood-Vasey, W. M. 2009, *AJ*, 138, 376
Frew, D. J. 2004, *Journal of Astronomical Data*, 10, 6
Gezari, S., Dessart, L., Basa, S., Martin, D. C., Neill, J. D., Woosley, S. E., Hillier, D. J., Bazin, G., Forster, K., Friedman, P. G., Le Du, J., Mazure, A., Morrissey, P., Neff, S. G., Schiminovich, D., & Wyder, T. K. 2008, *ApJL*, 683, L131
Hamuy, M., Phillips, M., Suntzeff, N., & Maza, J. 2003, *IAU Circ.*, 8151, 2
Hamuy, M. & Pinto, P. A. 2002, *ApJL*, 566, L63
Hillier, D. J., Davidson, K., Ishibashi, K., & Gull, T. 2001, *ApJ*, 553, 837
Hillier, D. J. & Miller, D. L. 1998, *ApJ*, 496, 407
Howell, D. A., Sullivan, M., Nugent, P. E., Ellis, R. S., Conley, A. J., Le Borgne, D., Carlberg, R. G., Guy, J., Balam, D., Basa, S., Fouchez, D., Hook, I. M., Hsiao, E. Y., Neill, J. D., Pain, R., Perrett, K. M., & Pritchett, C. J. 2006, *Nature*, 443, 308
Kitaura, F. S., Janka, H.-T., & Hillebrandt, W. 2006, *A&A*, 450, 345
Kochanek, C. S., Beacom, J. F., Kistler, M. D., Prieto, J. L., Stanek, K. Z., Thompson, T. A., & Yüksel, H. 2008, *ApJ*, 684, 1336
Kovetz, A. & Shaviv, G. 1994, *ApJ*, 426, 787
Kulkarni, S. R., Ofek, E. O., Rau, A., Cenko, S. B., Soderberg, A. M., Fox, D. B., Gal-Yam, A., Capak, P. L., Moon, D. S., Li, W., Filippenko, A. V., Egami, E., Kartaltepe, J., & Sanders, D. B. 2007, *Nature*, 447, 458
Leonard, D. C., Filippenko, A. V., Gates, E. L., Li, W., Eastman, R. G., Barth, A. J., Bus, S. J., Chornock, R., Coil, A. L., Frink, S., Grady, C. A., Harris, A. W., Malkan, M. A., Matheson, T., Quirrenbach, A., & Treffers, R. R. 2002a, *PASP*, 114, 35
Leonard, D. C., Filippenko, A. V., Li, W., Matheson, T., Kirshner, R. P., Chornock, R., Van Dyk, S. D., Berlind, P., Calkins, M. L., Challis, P. M., Garnavich, P. M., Jha, S., & Mahdavi, A. 2002b, *AJ*, 124, 2490

- Levesque, E. M., Massey, P., Olsen, K. A. G., Plez, B., Josselin, E., Maeder, A., & Meynet, G. 2005, *ApJ*, 628, 973
- Livne, E. 1993, *ApJ*, 412, 634
- Martins, F., Schaerer, D., & Hillier, D. J. 2005, *A&A*, 436, 1049
- Maund, J. R., Smartt, S. J., & Danziger, I. J. 2005, *MNRAS*, 364, L33
- Maund, J. R., Smartt, S. J., Kudritzki, R.-P., Pastorello, A., Nelemans, G., Bresolin, F., Patat, F., Gilmore, G. F., & Benn, C. R. 2006, *MNRAS*, 369, 390
- Mazzali, P. A., Deng, J., Maeda, K., Nomoto, K., Umeda, H., Hatano, K., Iwamoto, K., Yoshii, Y., Kobayashi, Y., Minezaki, T., Doi, M., Enya, K., Tomita, H., Smartt, S. J., Kinugasa, K., Kawakita, H., Ayani, K., Kawabata, T., Yamaoka, H., Qiu, Y. L., Motohara, K., Gerardy, C. L., Fesen, R., Kawabata, K. S., Iye, M., Kashikawa, N., Kosugi, G., Ohyama, Y., Takada-Hidai, M., Zhao, G., Chornock, R., Filippenko, A. V., Benetti, S., & Turatto, M. 2002, *ApJL*, 572, L61
- Meakin, C. A. & Arnett, D. 2006, *ApJL*, 637, L53
- Mihalas, D. 1978, *Stellar atmospheres /2nd edition/* (San Francisco, W. H. Freeman and Co., 1978. 650 p.)
- Mitalas, R. & Sills, K. R. 1992, *ApJ*, 401, 759
- Mocák, M., Müller, E., Weiss, A., & Kifonidis, K. 2008, *A&A*, 490, 265
- . 2009, *A&A*, 501, 659
- Murphy, J. W. & Burrows, A. 2008, *ApJ*, 688, 1159
- Nugent, P., Sullivan, M., Ellis, R., Gal-Yam, A., Leonard, D. C., Howell, D. A., Astier, P., Carlberg, R. G., Conley, A., Fabbro, S., Fouchez, D., Neill, J. D., Pain, R., Perrett, K., Pritchett, C. J., & Regnault, N. 2006, *ApJ*, 645, 841
- Owocki, S. P., Gayley, K. G., & Shaviv, N. J. 2004, *ApJ*, 616, 525
- Pastorello, A., Della Valle, M., Smartt, S. J., Zampieri, L., Benetti, S., Cappellaro, E., Mazzali, P. A., Patat, F., Spiro, S., Turatto, M., & Valenti, S. 2007, *Nature*, 449, 1
- Pastorello, A., Valenti, S., Zampieri, L., Navasardyan, H., Taubenberger, S., Smartt, S. J., Arkharov, A. A., Bärbantner, O., Barwig, H., Benetti, S., Birtwhistle, P., Botticella, M. T., Cappellaro, E., Del Principe, M., di Mille, F., di Rico, G., Dolci, M., Elias-Rosa, N., Efimova, N. V., Fiedler, M., Harutyunyan, A., Höflich, P. A., Kloeher, W., Larionov, V. M., Lorenzi, V., Maund, J. R., Napoleone, N., Ragni, M., Richmond, M., Ries, C., Spiro, S., Temporin, S., Turatto, M., & Wheeler, J. C. 2009, *MNRAS*, 394, 2266
- Pastorello, A., Zampieri, L., Turatto, M., Cappellaro, E., Meikle, W. P. S., Benetti, S., Branch, D., Baron, E., Patat, F., Armstrong, M., Altavilla, G., Salvo, M., & Riello, M. 2004, *MNRAS*, 347, 74
- Petit, V., Drissen, L., & Crowther, P. A. 2006, *AJ*, 132, 1756
- Poznanski, D., Butler, N., Filippenko, A. V., Ganeshalingam, M., Li, W., Bloom, J. S., Chornock, R., Foley, R. J., Nugent, P. E., Silverman, J. M., Cenko, S. B., Gates, E. L., Leonard, D. C., Miller, A. A., Modjaz, M., Serduke, F. J. D., Smith, N., Swift, B. J., & Wong, D. S. 2009, *ApJ*, 694, 1067
- Prieto, J. L., Kistler, M. D., Thompson, T. A., Yüksel, H., Kochanek, C. S., Stanek, K. Z., Beacom, J. F., Martini, P., Pasquali, A., & Bechtold, J. 2008, *ApJL*, 681, L9
- Richtmyer, R. D. & Morton, K. W. 1967, *Difference Methods for Initial Value Problems* (New York, Interscience 1967)
- Shaviv, N. J. 2000, *ApJL*, 532, L137
- Smartt, S. J. 2009, *ArXiv e-prints*
- Smith, N. 2008, *Nature*, 455, 201
- Smith, N., Ganeshalingam, M., Chornock, R., Filippenko, A. V., Li, W., Silverman, J. M., Steele, T. N., Griffith, C. V., Joubert, N., Lee, N. Y., Lowe, T. B., Mobberley, M. P., & Winslow, D. M. 2009a, *ApJL*, 697, L49
- Smith, N., Gehrz, R. D., Hinz, P. M., Hoffmann, W. F., Hora, J. L., Mamajek, E. E., & Meyer, M. R. 2003, *AJ*, 125, 1458
- Smith, N., Hinkle, K. H., & Ryde, N. 2009b, *AJ*, 137, 3558
- Smith, N., Li, W., Foley, R. J., Wheeler, J. C., Pooley, D., Chornock, R., Filippenko, A. V., Silverman, J. M., Quimby, R., Bloom, J. S., & Hansen, C. 2007, *ApJ*, 666, 1116
- Smith, N. & McCray, R. 2007, *ApJL*, 671, L17
- Utrobin, V. P. 2007, *A&A*, 461, 233
- Utrobin, V. P. & Chugai, N. N. 2008, *A&A*, 491, 507
- . 2009, *ArXiv e-prints*
- Valenti, S., Pastorello, A., Cappellaro, E., Benetti, S., Mazzali, P. A., Manteca, J., Taubenberger, S., Elias-Rosa, N., Ferrando, R., Harutyunyan, A., Hentunen, V. P., Nissinen, M., Pian, E., Turatto, M., Zampieri, L., & Smartt, S. J. 2009, *Nature*, 459, 674
- Van Dyk, S. D., Peng, C. Y., King, J. Y., Filippenko, A. V., Treffers, R. R., Li, W., & Richmond, M. W. 2000, *PASP*, 112, 1532
- Weaver, T. A. & Woosley, S. E. 1979, in *Bulletin of the American Astronomical Society*, Vol. 11, *Bulletin of the American Astronomical Society*, 724+
- Woosley, S. E., Blinnikov, S., & Heger, A. 2007a, *Nature*, 450, 390
- Woosley, S. E., Eastman, R. G., & Schmidt, B. P. 1999, *ApJ*, 516, 788
- Woosley, S. E., Heger, A., & Weaver, T. A. 2002, *Reviews of Modern Physics*, 74, 1015
- Woosley, S. E., Kasen, D., Blinnikov, S., & Sorokina, E. 2007b, *ApJ*, 662, 487
- Zeldovich, Y. B. & Novikov, I. D. 1971, *Relativistic astrophysics. Vol. I: Stars and relativity*, ed. Y. B. Zeldovich & I. D. Novikov